SLAC-PUB-3015
November 1982
(T/E)

Conf-821079--3

Quark-Antiquark Bound-State Spectroscopy and QCD

E. D. Bloom

Stanford Linear Accelerator Center
Stanford University, Stanford, California 94305

SLAC-PUB--3015

DE83 007062

*Work supported by the Department of Energy, contract DE-AC03-76SF00515.

Presented at the 9th SLAC Summer Institute on Particle Physics, Stanford, CA, July 27 - August 7, 1981.

Quark-Antiquark Bound State Spectroscopy and QCD

I. Introduction.

Spectroscopy is the study of the energy levels of a bound system and the transitions among these levels. Frequently it has not been clear that the states and transitions being observed were a realization of an underlying substructure. In this initial phase of study the different particle states were organized into "understandable" patterns, e.g., SU(2), SU(3), Color, which then led to a deeper understanding.

There are at least two important uses of spectroscopic investigations. The first is the search for new substructure. Consider for example, the emergence of the quark substructure of the hadrons. In the late 1950's the $\Delta(1238)$, with $I=3/2$, had not yet been discovered, and so one finds this statement in a well known textbook published in 1959: "Let us now see what kinds of particle types can be formed by various choices of [I], A, and S, bearing in mind that no experimental evidence has yet indicated the existence of multiple charges for elementary particles." The fact that the observed hadron charges at that time were $0, \pm 1$, was made into a general rule for interpreting the underlying physics, and orgainizing all states. Thus, as has been stated by D. H. G. S. Leith, knowledge of the "chessmen," the constituents characterized by their quantum numbers, is one important aim of spectroscopy.

The second important use of spectroscopy is the unraveling of the

dynamics of a new substructure once it has been discovered. This effort encompasses determining the equations of motion and the forces which govern the substructure. Its final outcome will be a detailed understanding of the spectroscopy which led to the postulation of a substructure in the first place. The most successful past efforts of this type have used non-relativistic bound systems to explore the equations of motion and the forces, e.g., the study of the hydrogen atom. Thus the excitement generated by the discovery of Quarkonium, $q\bar{q}$ bound states in which the excitations of the constituent heavy quarks is a small fraction of their rest mass, is clearly justified. Through the careful study of the spectroscopy of these quark-antiquark bound systems we shall almost certainly gain a deep understanding of quark dynamics.

II. The Search For The Chessmen.

a). The Quarks As We Now Know Them. After almost four decades of intensive work the properties of the constituents of hadrons can with fair certainty be enumerated as shown in table 1.

Flavors Quantum #	d	u	s	c	b
I	$\frac{1}{2}$	$\frac{1}{2}$	0	0	0
I_z	$-\frac{1}{2}$	$\frac{1}{2}$	0	0	0
Q	-1/3	2/3	-1/3	2/3	-1/3
S(Strangeness)	0	0	-1	0	0
C(Charmness)	0	0	0	1	0
B(Bottomness)	0	0	0	0	1
Approximate Constituent mass (MeV)	350	350	500	1500	4900

Table 1. The quarks as we now know them.

Each quark listed in the table comes in three colors, red (R), blue (B) and yellow (Y). Thus the table repesents 15 quarks. The top quark is also expected, but has a mass $\geq$ 18.5 GeV[1]. Consideration of quark-lepton symmetry, and the GIM model[2] for charm, leads one to organize the quarks and leptons into three groups or generations.

Generation 1		Generation 2		Generation 3	
$\begin{pmatrix} u \\ d' \end{pmatrix}$	$\begin{pmatrix} \nu_e \\ e^- \end{pmatrix}$	$\begin{pmatrix} c \\ s' \end{pmatrix}$	$\begin{pmatrix} \nu_\mu \\ \mu^- \end{pmatrix}$	$\begin{pmatrix} ? \\ b' \end{pmatrix}$	$\begin{pmatrix} \nu_\tau \\ \tau^- \end{pmatrix}$

Table 2. The three generations of leptons and quarks. Note that the three generations contain 24 elementary particles. ? is presumably the top quark, t.

Some remarks are in order. The organization shown in table 2 into three generations of pairs of [SU(2) x U(1)] doublets (weak isospin) seems fundamental. The success of weak isopspin implies that strong I-spin symmetry, $SU(2)_f$, is an accident of nature resulting from the almost degenerate masses of the u and d quarks. Also, the approximate validity of $SU(3)_f$ is due to the closeness of the s quark mass to the u and d quark masses. Thus, the old way of viewing the strong interactions is not fundamental from the perspective of QCD. $SU(4)_f$ and $SU(5)_f$ are even less fundamental given the large mass differences of the b, c, to the u, d, and s quarks. What makes $SU(n)_f$ work so well is the apparent flavor independence of the $q\bar{q}$ force for mesons and the qqq force for baryons. The flavor independence of these forces is certainly fundamental (if true). However, the flavor independence of inter-quark forces is called into question in the beautiful lectures given by H. Harari at the S.L.A.C. Summer Institute of 1977[3]. As stated by Harari, "There is no explanation whatsoever for the $\mu - e$, $c - u$, and $s - d$ mass differences. While the $\nu_e - e$ and $\mu - d$ mass differences may well be of electromagnetic origin, the $\nu_\mu - \mu$ and $c - s$ differences are larger by 2 - 3 orders of magnitude. The

ν_e - e and u-d differences are essentially comparable order of magnitude and equal in sign. the ν_μ - μ and c - s differences are of different orders of magnitude and of opposite signs." In the context of present ideas, this suggests a new force which is flavor dependent.

b). The Classification of Ordinary Mesons in Terms of Constituent Quarks.

In these lectures we will concentrate on the $q\bar{q}$ system. There are at least two reasons to do this. Firstly, the $q\bar{q}$ system is a two body system and so its dynamics can be modeled with relative ease. This is not true for the qqq system which is a three body system having well known calculational difficulties. Systems with more than three constituent quarks present even graver difficulties. Secondly, in recent years much has been learned about the $q\bar{q}$ system through the discovery of the c - and b - onia, as well as through many discoveries of new particle states of the light mesons. Progress with the qqq spectrum has been much slower. Thus I refer the interested reader to the literature for a review of the qqq system[4].

Given the bias of history we begin with the "non-fundamental" group theoretical approach in considering mesons whose constituents are pairs of u, d, and s quarks and antiquarks. These are the "ordinary" mesons. The spin $\frac{1}{2}$ q and $\bar{q}$ lie in a 6 and $\bar{6}$ representation of SU(6) (u, d, s x 2 spin states). For a $q\bar{q}$ system,

$$6 \otimes \bar{6} = 1 \oplus 35 \qquad \text{(II-1)}$$

The 1 and 35 representations of SU(6) can be decomposed into $SU(3)_f$ and $SU(2)_{spin}$ components where we use the notation,

$$(SU(3)_f,\ 2s+1), \qquad \text{(II-2)}$$

s being the spin of the particles belonging to the $SU(2)_{spin}$ representation. We then obtain the decomposition into irreducible representations shown in table 3.

SU(6)	$(SU(3)_f, 2s+1)$
1	(1,1)
35	(8,1),(8,3),(1,3)

Table 3. $SU(6) \rightarrow SU(3)_f \otimes SU(2)_{spin}$

Also, for each $(SU(3)_f, 2s+1)$ representation, there are orbital excitations and radial excitations (V(r) from QCD).

A considerably more transparent way to obtain the same result is to take the $q\bar{q}$ model seriously. Figure 1 shows the essence of the model considered here. The q and $\bar{q}$ are bound non-relativistically by a potential, V(r). Part a) of the figure shows the singlet spin state configuration, part b) shows one of the three triplet states.

In approximating the structure of mesons using this simple model, the strong forces between the q and $\bar{q}$ arise from color electric and color magnetic fields. There is no known way to apply an external field of these types, so the consideration of the magnetic quantum number , m, can be dropped when writing the wave function for the system. Thus, the wave function for the system can be written as follows.

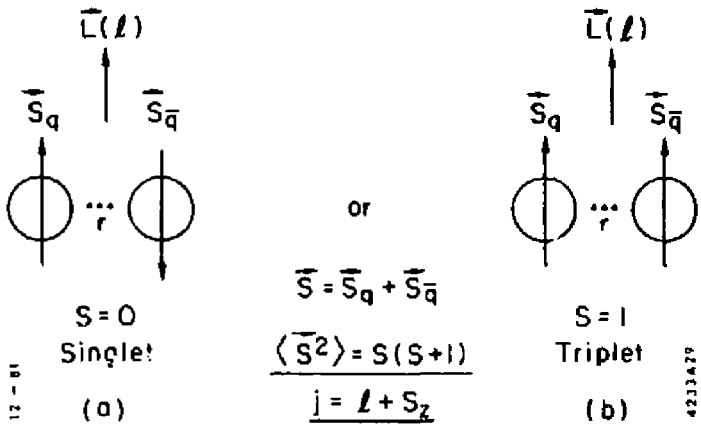

Figure 1. The non-relativistic quark model for mesons.
a). Single State. b). One of the Triplet States.

$$|q\bar{q}\rangle \propto \bar{R}_n(r)\, P_\ell^{s_z}(\cos\theta)\, |2s+1, s_z\rangle\, \Psi_f\, \Psi_c, \qquad \text{(II-3)}$$

where n is the principle quantum number, $\ell = 0, 1, \ldots (n-1)$ is the orbital angular momentum quantum number, $s = 0, 1$ for singlet and triplet states respectively, $s_z = 0, \pm 1$, $j = \ell + s_z$ is the total angular momentum quantum number, Ψ_f is the $SU(3)_f$ factor in the wave function (for ordinary mesons), and Ψ_c is a color SU(3) singlet as dictated by quark confinement,

$$\Psi_c = (R\bar{R} + B\bar{B} + Y\bar{Y})/\sqrt{3}\ , \qquad \text{(II-4)}$$

The spin eigenstates, $|2s+1, s_z\rangle$, are given in terms of the individual quark and antiquark spin eigenstates by,

$$\text{Singlet: } |0,0\rangle = (|\tfrac{1}{2},\tfrac{1}{2}\rangle_q|\tfrac{1}{2},-\tfrac{1}{2}\rangle_{\bar{q}} - |\tfrac{1}{2},-\tfrac{1}{2}\rangle_q|\tfrac{1}{2},\tfrac{1}{2}\rangle_{\bar{q}})/\sqrt{2}$$

$$\text{Triplet: } |1,s_z\rangle = \begin{cases} |\tfrac{1}{2},\tfrac{1}{2}\rangle_q|\tfrac{1}{2},\tfrac{1}{2}\rangle_{\bar{q}} \\ (|\tfrac{1}{2},\tfrac{1}{2}\rangle_q|\tfrac{1}{2},-\tfrac{1}{2}\rangle_{\bar{q}} + |\tfrac{1}{2},-\tfrac{1}{2}\rangle_q|\tfrac{1}{2},\tfrac{1}{2}\rangle_{\bar{q}})/\sqrt{2} \\ |\tfrac{1}{2},-\tfrac{1}{2}\rangle_q|\tfrac{1}{2},-\tfrac{1}{2}\rangle_{\bar{q}} \end{cases} \qquad \text{(II-5)}$$

The label of the state in spectroscopic notation is,

$$n^{2s+1}\ell_j^{PC} \qquad \text{(II-6)}$$

where we shall use the standard spectroscopic notation, $\ell = 0, 1, 2, \ldots \rightarrow$ S, P, D, ..., and again, $s = 0, 1$, and, $j = \ell + s_z$.

As can be shown[5], the parity, P, and charge conjugation, C, of the $q\bar{q}$ system are given by,

$$P = -(-1)^{\ell} \qquad \text{(II-7)}$$

$$C = (-1)^{\ell+s}\ . \qquad \text{(II-8)}$$

Except for flavor, this simple model yields the following set of states.

$$\text{Singlet: } n^1J_L = \epsilon(-1)^{\theta}\cdot\epsilon(-1)^{\phi} \qquad \text{(II-9)}$$

$$\text{Triplet: } n^3J_{L-1} = \epsilon(-1)^{\theta}\cdot\epsilon(-1)^{\phi+1},$$

$$n^3J_L = \epsilon(-1)^{\gamma}\cdot\epsilon(-1)^{\zeta+1},$$

$$n^3J_{L+1} = \epsilon(-1)^{\zeta}\cdot\epsilon(-1)^{\mu+1}.$$

As we shall see, essentially all the known mesons can be classified in this way.

The flavor content of the wave function can be determined in two ways. The old fashioned way is to use SU(3)$_f$ as is shown in table 4.

meson generic type	Quark Flavor states	SU(2)$_f$ representation	SU(3)$_f$ representation
π^+ ,π^0 , π^-	$d\bar{u}$, $(u\bar{u}-d\bar{d})/\sqrt{2}$, $u\bar{d}$	3	
K^+ , K^0	$u\bar{s}$, $d\bar{s}$	2	8
$\bar{K}^0$, K^-	$s\bar{d}$, $s\bar{u}$	2	
η^0	$(u\bar{u}+d\bar{d}-2s\bar{s})/\sqrt{6}$	1	
η'^0	$(u\bar{u}+d\bar{d}+s\bar{s})/\sqrt{3}$	1	1

Table 4. SU(3)$_f$ Multiplets for the ordinary hadrons.

However, the singlet SU(2)$_f$ states, of the SU(3)$_f$ 8 and 1 representations, frequently mix (magic mixing) to make the physical meson states almost diagonal in quark flavor; i.e.,

$(u\bar{u}+d\bar{d}+s\bar{s})/\sqrt{3}$	MIX →	$(u\bar{u}+d\bar{d})/\sqrt{2}$	(II-10)
$(u\bar{u}+d\bar{d}-2s\bar{s})/\sqrt{6}$		$s\bar{s}$	
SU(3)$_f$ states		Physical states	

This experimental fact, coupled with the structure of SU(6), has led to the grouping of the 8 and 1 representations of SU(3)$_f$ into "nonets" of mesons.

Another, more physically motivated, way to obtain the flavor wave functions is to use the inferred masses of the light quarks, i.e. $m_u \approx m_d < m_s$. Using our simple $q\bar{q}$ model of meson structure, only the following 9 flavor states exist for the ordinary mesons:

$u\bar{u}$	$d\bar{u}$	$s\bar{u}$	9 flavor states	(II-11)
$u\bar{d}$	$d\bar{d}$	$s\bar{d}$		
$u\bar{s}$	$d\bar{s}$	$s\bar{s}$		

Since $m_u \approx m_d$, and we have at least approximate flavor independence of the QCD forces, we expect $u\bar{u}$ and $d\bar{d}$ to optimally mix, and so the physical states involving $u\bar{u}$ and $d\bar{d}$ will be,

$$(u\bar{u} + d\bar{d})/\sqrt{2} \ , \ (u\bar{u} - d\bar{d})/\sqrt{2} \ . \qquad \text{(II-12)}$$

The $s\bar{s}$ state typically won't mix since m_s is quite a bit larger than the u and d quark masses. We then use $SU(2)_f$ and strangeness (observation) to assign particle types to the appropriate flavor wavefunction. The results obtained using $SU(3)_f$ + magic mixing are thus duplicated in a somewhat less "magic" way.

Using all the elements of the simple model we have developed, a classification of all the observed ordinary meson states can be attempted. The results of such an attempt by Roger Chashmore[9] (slightly modified) is shown in figure 2; it is quite successful. Most of the observed ordinary mesons can be classified using the simple $q\bar{q}$ model I have described.

The search for mesons whose quantum numbers don't satisfy the (P, C) $\rightarrow$ (P, C) relationships of equations (II-7) and (II-8), so-called exotic mesons, has not yielded any convincing candidates, also, exotic mesons of the type having S = -1 and Q = 1 have not been found. However, there may exist evidence for a deviation from the simple $q\bar{q}$ classification in the 0^{++} mesons spectrum. At present the following 0^{++} ordinary mesons have been identified[9]: δ(1300,300), ϵ(1425,160), χ(1500,=250), δ(980,narrow), ϵ(=800,large), S^*(=990,narrow), where the first number in the parentheses is the mass of the state in MeV and the second entry is the width. These states are all $2^3P_0^{++}$ candidates (shown as "needs confirmation" in figure 2). The $n^3P_j^{++}$ states should be close in mass, for fixed n, for a non-relativistic $q\bar{q}$ system. This is because the spin-orbit interaction of the $q\bar{q}$ is the mechanism for this mass splitting, and it is supposed to be a small perturbation in the mass, i.e., fine structure. The first three states listed satisfy the criterion of small splitting from the other 2^3P_2 and 2^3P_1 states, and so are very likely $q\bar{q}$ states with 2^3P_0. However, the

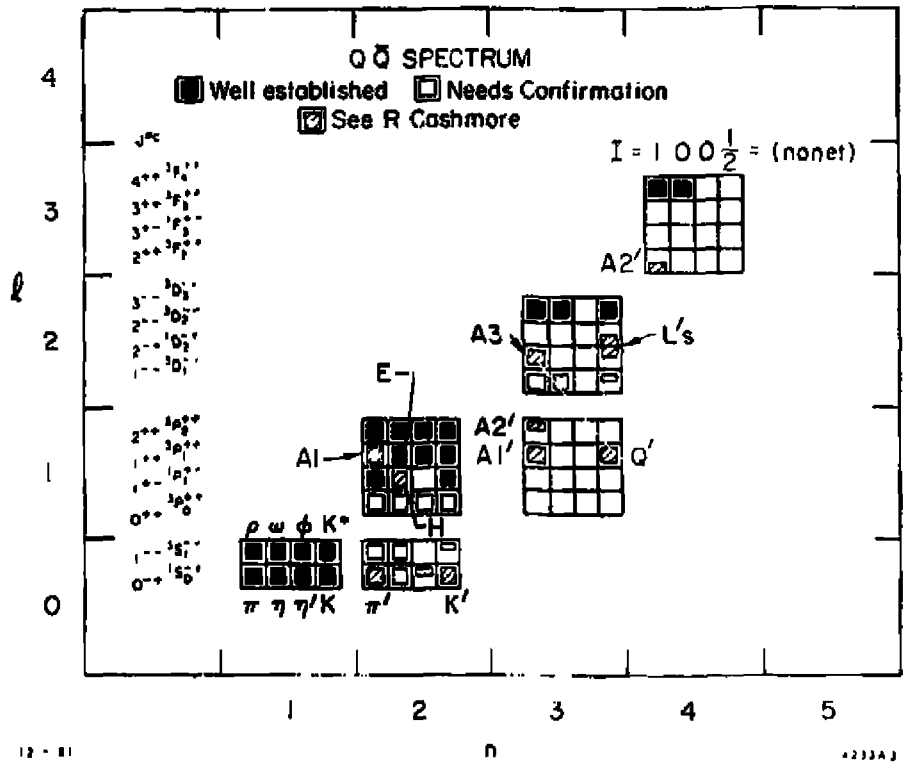

Figure 2. The observed ordinary meson spectrum classified using the non-relativistic $q\bar{q}$ model developed in the text. ℓ vs n (Principle quantum number).

last three states listed lie much lower in mass than the other 2^3P_j states, $\Delta m/\langle m\rangle \approx 0.35$; for charmonium the 2^3P_j states satisfy $\Delta m/\langle m\rangle \approx 0.02$. The explanation for this is presently controversial. My feeling is that the ordinary mesons are really quite relativistic $q\bar{q}$ systems and thus the non-relativistic treatment of the spin-orbit interaction, and other non-relativistic approximations made, are not applicable to these states (*garbage in, garbage out*). Others, such as Jaffe and Low, believe a more acceptable explanation requires the existence of a new set of $q\bar{q}q\bar{q}$ states which they have predicted. They call these 0^{++} $q\bar{q}q\bar{q}$ states "cryptoexotics." Note that the cryptoexotic states are a complication, rather than a reformation, of the $q\bar{q}$ model.

c). Hidden Charm States and Charmed Mesons.

With the discovery of the $c\bar{c}$ system, charmonium, the predictive power of the simple non-relativistic $q\bar{q}$ model can finaly be tested under realistic conditions. This can easily be seen through the application of two basic principles, the virial theorem and conservation of energy. For a non-relativistic system, where the binding force can be expressed through a potential, the virial theorem can be stated as,

$$2\langle T\rangle = \langle \vec{r}\cdot\vec{\nabla}V(r)\rangle \ . \qquad (II\text{-}13)$$

The conservation of energy is given by,

$$\langle T\rangle + \langle V\rangle = E_b \ . \qquad (II\text{-}14)$$

In the above equations, T is the kinetic energy of the system, V(r) is the potential between the q and $\bar{q}$ separated by r; E_b is the binding energy. For V(r) $\propto$ r (confining potential which we discuss later), we obtain,

$$2\langle T\rangle = \langle V(r)\rangle, \qquad \text{(II-15)}$$

and so,

$$\langle T\rangle = E_b, \text{ or, } m_q\langle v^2\rangle = E_b/3, \qquad \text{(II-16)}$$

where v^2 is the square of the q ($\bar{q}$) velocity.

For ordinary mesons, states are quasibound at the 1^3S_1 level,

$$E_b \simeq m(1^3S_1) - m(1^1S_0) \simeq 600 \text{ MeV}, \qquad \text{(II-17)}$$

$$\langle v^2\rangle \simeq 600/1050 \simeq 0.6. \qquad \text{(II-18)}$$

The full calculation using,

$$V(r) = k\log(r/r_0) \qquad \text{(II-19)}$$

yields, $\langle v^2\rangle \simeq 1$. The general formula for the potential (II-19) is[7],

$$\langle v^2\rangle = k/2m_q, \; k \simeq 0.75 \qquad \text{(II-20)}$$

In the case of hidden charm states, $c\bar{c}$ threshold is at the 3^3D_1 state, and our simple analysis yields,

$$E_b = m(3^3D_1) - m(1^1S_0) = 888 \text{ MeV}, \qquad (II-21)$$

$$\text{or, } \langle v^2 \rangle = 800/4500 = 0.18. \qquad (II-22)$$

Equation (II-20) yields, $\langle v^2 \rangle = 0.25$. Thus the $c\bar{c}$ system can be treated in reasonable approximation as non-relativistic, while ordinary mesons are clearly quite relativistic systems.

Predicting the states for charm is straightforward (measuring them is another question). Either SU(4)$_f$ can be used, as shown in figure 3, or one can simply quark count.

The hidden charm and charmed meson spectrum is shown in figure 4 a, b. As we shall discuss later, most of the low-lying states which have been predicted have been observed, and at close to the predicted masses.

d). Add Bottom Quarks.

In the case of the $b\bar{b}$ system, with $m_b \approx 5$ GeV, the non-relativistic approximation is quite good. For this case, the bound state spectrum extends to the 4^3S_1 state.

$$E_b = m(4^3S_1) - m(1^1S_0) = 1200 \text{ MeV}, \qquad (II-23)$$

and, $\langle v^2 \rangle = 1200/15000 = 0.08$, the value also obtained using equation (II-20). We will discuss the $b\bar{b}$ system in some detail later in these

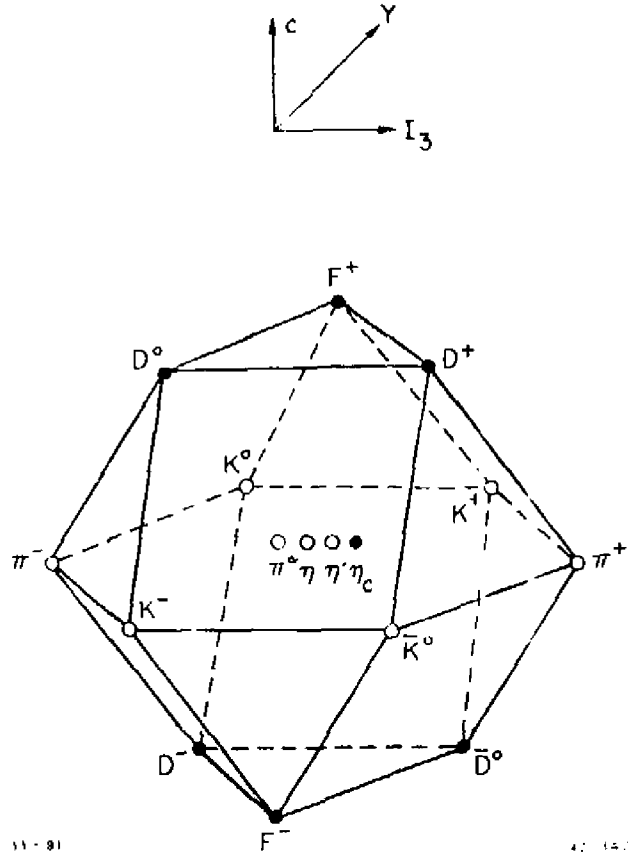

Figure 3. The hexadecimet of the pseudoscalar mesons. Charm is plotted along the z-Axis , Y and I_z along respectively the y-Axis and the x-Axis. The π^0, η and η' mesons are denoted by the open circles at the origin, η_c by the black circle.

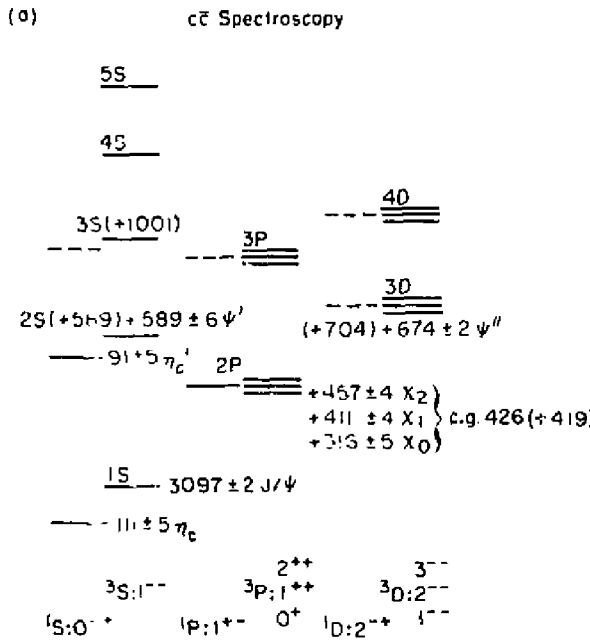

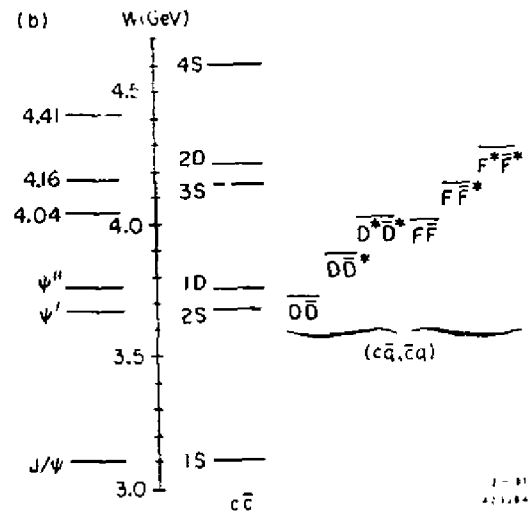

Figure 4a. The cc̄ spectrum together with the experimental values of mass differences, the theoretical predictions of J. F. Richardson[8] are in parentheses. (Note that c.g. = center of gravity or cog, c.f. section IV-d).

Figure 4b. The cc̄ levels, the lowest lying charmed meson channels and the measured position of vector mesons[9].

lectures. Figure 5 shows the incredibly rich bound state spectroscopy (all states below 4s are probably bound) which should exist.

III. The Interquark Forces and the Particle Spectrum.

a). The e^+e^- Bound System, Positronium, a Model for $q\bar{q}$.

Positronium was predicted in 1934 by the well known Croatian (astro-) physicist, S. Mohorovicic[9]. It was first observed in experiments performed by M. Deutch[10] in 1951. The ^3o_j states were first seen by Mills, Berko and Canter[11] in 1975, and the $2^3S_1 - 2^3P_2$ fine structure was measured. This measurement verified the QED predictions of Fulton and Martin[12] made in 1954. The time scale of charmonium looks instantaneous by comparison.

Positronium is a non-relativistic QED bound state of an e^+ and an e^-; that it is non-relativistic is easy to show. For positronium,

$$V(r) = -\alpha/r, \quad E_b^n = -6.8/n^2 \text{ eV}. \qquad \text{(III-1)}$$

Using equations (II-13) and (II-14) we find,

$$2\langle T\rangle = -\langle V(r)\rangle, \rightarrow \langle v^2\rangle \approx 6.8/5.11\times10^5 = 1.3\times10^{-5}. \qquad \text{(III-2)}$$

Even though positronium is super non-relativistic, a variant of the Dirac equation plus other relativistic corrections are needed to obtain the

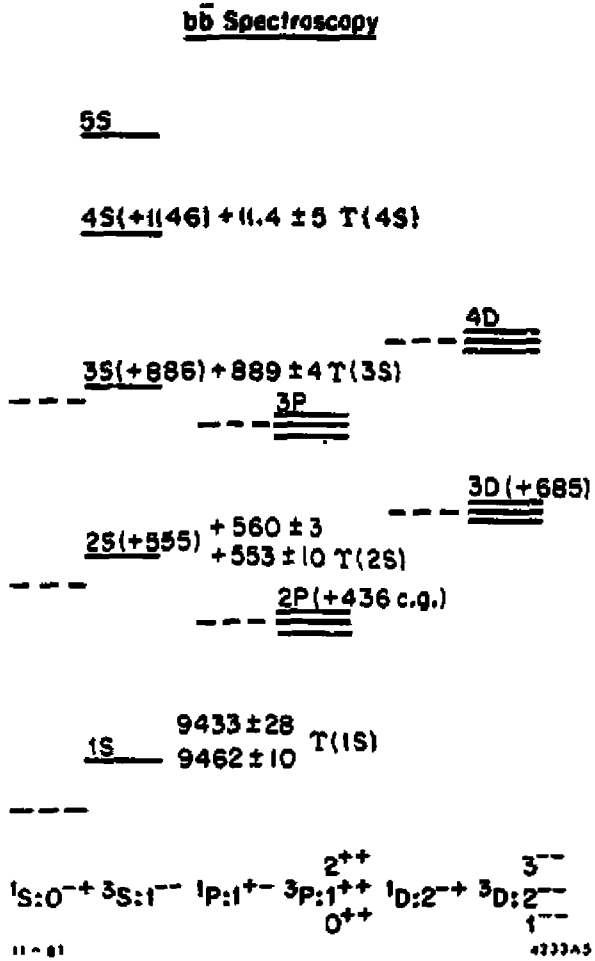

Figure 5. The $b\bar{b}$ spectrum together with the experimental values of mass differences. the theoretical predictions of J.R. Richardson[8] are in parentheses.

fine structure and hyperfine structure in lowest order. This is because the fine structure splitting of the nS - nP states involves spin-orbit interactions including the so called "Thomas precession" term (a relativistic kinematic effect which is linear in v). Also, the hyperfine splitting of the n^3S_1 - n^1S_0 states involves an annihilation d agram in positronium, beside the usual spin-spin interaction.

The equation used is called the Groutch-Yennie-Dirac equation[13]. This equation is basically the Dirac equation modified by G-Y to include relativistic two body kinematics[14]. With this equation accurate fine-structure splitting is obtained. The hyper-fine splitting is obtained by including as a perturbation the diagrams shown in figure 6.

Note that the f-s obtained is, $f\text{-}s/\Delta E_n \approx 4\times10^{-6}$, while the hf-s is larger for positronium, $hf\text{-}s/\Delta E_n \approx 10^{-5}$, (this is reversed for the hydrogen atom).

The decay pattern of positronium into photons is deterained by the j^{PC} of each state[15],

$$\begin{aligned} &n^1S_0 \rightarrow 2\gamma \\ &n^3S_1 \rightarrow 3\gamma. \\ &n^3P_2,\ n^3P_0 \rightarrow 2\gamma \\ &n^3P_1 \rightarrow 4\gamma,\ (n^3P_1 \rightarrow \gamma + (n-1)^3S_1(3\gamma)) \end{aligned} \qquad \text{(III-3)}$$

The $^1S_0$ decay is easy to calculate; referring to figure 7,

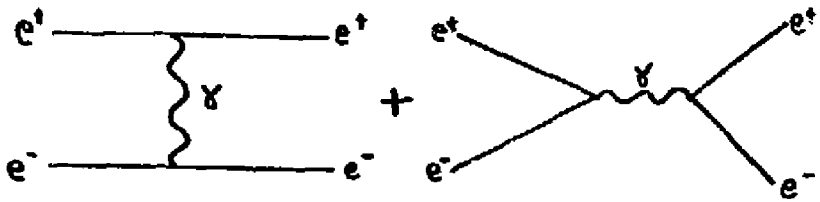

Figure 6. The diagrams used to calculate the hyper-fine splitting for positronium.

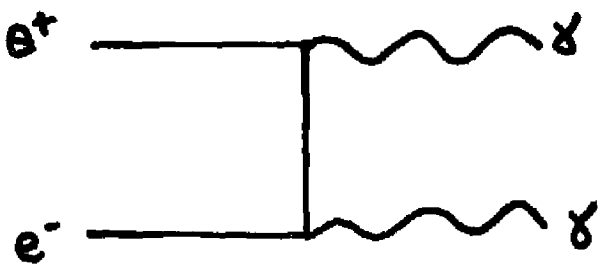

Figure 7. Diagrammatic representation of the decay $^1S_0 \rightarrow 2\gamma$.

$$\Gamma(^1S_0 \to 2\gamma) = \text{(probability of } e^+e^- \text{ contact)} * (\sigma_{\gamma\gamma}(v_{rel} \to 0)) * \text{(flux factor)} * \text{(statistical factor)} \qquad \text{(III-4)}$$

The first factor in (III-4), the probability of e^+e^- contact, is just $|\Psi(0)|^2$, the square of the wave function at the origin. The second is the e^+e^- annihilation cross section to 2γ taken in the limit of small $e^\pm$ relative velocity, v_{rel},

$$\sigma_{\gamma\gamma}(v_{rel} \to 0) = \pi(\alpha^2/m_{e^\pm}^2)/v_{rel} \qquad \text{(III-5)}$$

The flux factor is just v_{rel}, and so, $\sigma_{\gamma\gamma} \times v_{rel}$ is the transition probability for the annihilation process with the "beam" normalized to one particle per unit volume at the origin.

The statistical factor has the value 4, since $\sigma_{\gamma\gamma}$ has been obtained as an average over the initial e^- and e^+ spins and only the $^1S_0$ and not the three $^3S_1$ states contribute to the 2γ decay of positronium.

The result of combining all the factors of equation (III-4) is,

$$\Gamma(^1S_0 \to 2\gamma) = 16\pi\alpha^2|\Psi(0)|^2/m_{e^\pm}^2 \qquad \text{(III-6)}$$

The $^1S_1 \to 3\gamma$ decay is more difficult to calculate. The rate of this decay is much lower than (III-6) due to two factors. The first is an extra factor of α due to the emission of a third photon; this lowers the rate by a factor of ≈ 137. The second factor, of about another 8 reduction in rate, comes from the smaller available phase space of the three photon (as

compared to the two photon) final state. The formula for this positronium decay is given by[15],

$$\Gamma(^3S_1 \rightarrow 3\gamma) = 64(\pi^2-9)\alpha^3|\Psi(0)|^2/9m_{e\bar{e}}^2 \qquad \text{(III-7)}$$

Comparing (III-6) to (III 7) we find,

$$\Gamma(^3S_1 \rightarrow 3\gamma) = 8.98\times10^{-3}\Gamma(^1S_0 \rightarrow 2\gamma) \qquad \text{(III-8)}$$

Figure 8 shows the calculated energy levels and values of $1/\Gamma$ for the n=2 levels of positronium.[15]

The features of the spectrum shown in figure 8 relevant to the case of charmonium are:

- The size of the splittings relative to the principal quantum number energy differences.
- The relative size of the fine and hyperfine splitting.
- The pattern of the splitting.
- The lifetimes of the C = + vs. C = - states.

The last three features bear an uncanny resemblance to charmonium. One should note, however, that the center of gravity, cog, of the 2^3P_j states is shifted below the unperturbed value of $1/3\ ^3P_J$. This is not the case for the hydrogen atom, and is currently assumed not to be the case for the $q\bar{q}$ system.

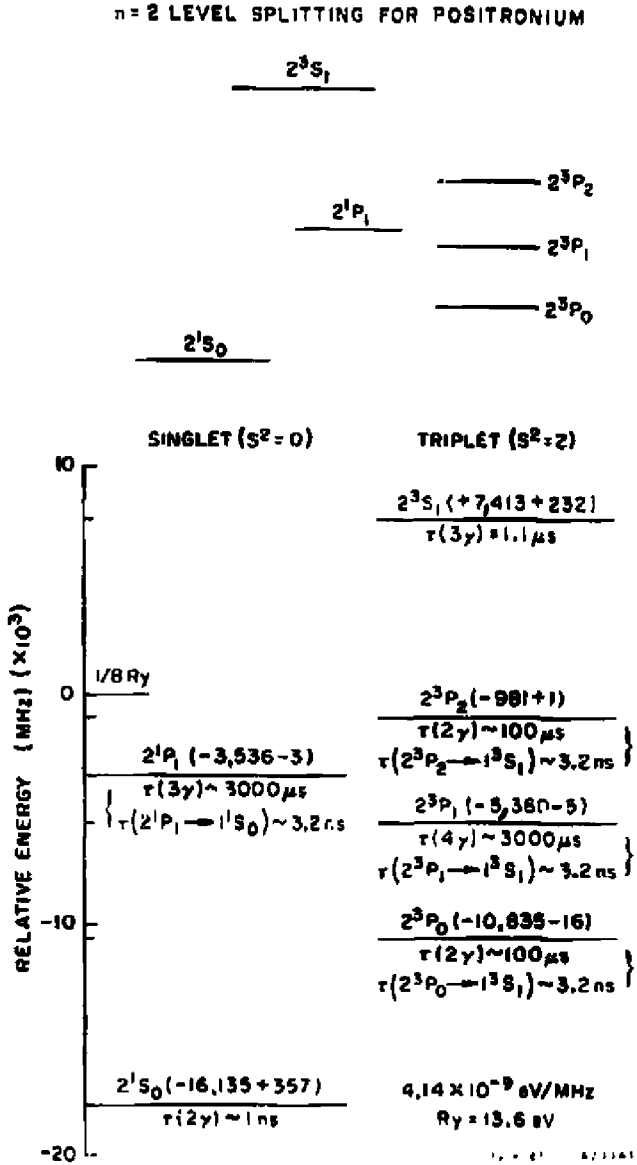

Figure 8 The n = 2 level structure of positronium. The numbers in parentheses represent the $O(\alpha^3)$ [illegible] and $O(\alpha^5)$ (radiative corrections) to the fine energy level ($1/8^2$ Ry). [illegible] For example, these corrections to 2^1P_1 are -3.36 GHz = -3 MHz, respectively.

b). QCD and its Foundation in Experiment.

Quantum Chromodynamics is the candidate theory for the strong interactions[16]. It is a gauge theory under the group $SU(3)_{color}$. We thus believe that the color quantum number of the quarks is the charge of the new force which is generated by a local gauge group, $SU(3)_{color}$. QCD is non-abelian, i.e, the transmitters of the color force, massless spin one gluons, also carry the color charge.

There are several reasons based on experiment to believe that there is a global $SU(3)_{color}$ symmetry:

- The rate for $\pi^0 \rightarrow 2\gamma$. The calculated decay rate is wrong by a factor of 9 without color; with color included, $\Gamma_{exp} = 7.86 \pm 0.54$ eV[17], compares well to the theoretical value of, $\Gamma_{theory} = 7.3$ eV[18].
- The baryon wave function. With color, the ground states of baryons can be understood in the quark model, without abandoning the connection between spin $\frac{1}{2}$ and Fermi-Dirac statistics. In the case of the Ω^-, for example, there are three s quarks in an orbital $\ell = 0$ state with all spins aligned. This spatial-spin configuration has a symmetric wavefunction, and, the Ω^- can't have a 1/2 spin (as it does) if consistency with spin-statistics is required. With three colors, however, overall anti-symmetry can be restored to the wavefunction if the Ω^- is made a color singlet; happily, the color singlet wavefunction of three quarks is antisymmetric.

- $R_h = \sigma_{tot}(e^+e^- \to \text{hadrons})/\sigma(e^+e^- \to \mu^+\mu^-)$.

  Using the free quark model without color, R_h^0 is just the sum of the squares of the quark electric charges, e.g., at $E_{cm} \approx 7$ GeV, $R_h^0 = 2(1/3)^2 + 2(2/3)^2 = 10/9$. If we add the color charge, $R_h = 3 \times R_h^0 = 10/3$. The experimentally determined value at ≈ 7 GeV is[19] $R_h = 4.0 \pm 0.32$. Clearly, the color charge is again needed to obtain reasonable agreement with experiment.

These experimental comparisons don't check the local $SU(3)_{color}$ gauge invariance, they just check a global $SU(3)_{color}$ symmetry. It is generally harder to check the local gauge symmetry, since experimental effects involve higher order QCD (quark "structure"). R_h can be used as a check of the local gauge invariance because higher order QCD affects R_h[20]. (there are quark structure effects due to quark-gluon virtual interactions). To second order,

$$R_h = 3\sum_{i=1}^{n_f} Q_i^2(1+\alpha_s(s)/\pi+C_2(\alpha_s(s)/\pi)^2+\cdots) \qquad \text{(III-9)}$$

where, $s = E_{cm}^2$, n_f = # flavors above threshold,

$$C_2 = 1.98 - 0.115n_f \ , \qquad \text{(III-10)}$$

$$\alpha_s(s) = \alpha_s^0(s)[1-\beta_1\alpha_s^0(s)\ln\ln(s/\Lambda^2)/4\pi\beta_0+\cdots] \qquad \text{(III-11)}$$

$$\alpha_s^0(s) = 4\pi/(\beta_0\ln(s/\Lambda^2)), \qquad \text{(III-12)}$$

$$\beta_0 = 11 - 2/3n_f, \ \beta_1 = 102 - (38/3)n_f \qquad \text{(III-13)}$$

The above expressions have been obtained using QCD with the $\overline{MS}$ renormalization scheme[20], and n_f is the number of light quarks (3 in the case of the energies shown for R_h). Λ is an undetermined scale parameter in the theory. Thus $SU(3)_{color}$ as a local gauge theory does have observable effects, even though they are difficult to observe, $\Delta R_h \approx 10\%$. Figure 9 shows a summary of R_h measurements vs the predictions of equations (III-9) – (III-13).

Another place to test QCD is in deep inelastic lepton hadron scattering, $\ell^{\pm} + N \rightarrow \ell^{\pm} + X$, where only the final state lepton ($\ell^{\pm}$) is detected. This process is viewed as the scattering of the high energy lepton from the quasi-free quark constituents of the nucleon. Neglecting QCD the quarks would act as point charges; the higher order effects of QCD cause a smearing of the quark charge and the scattering deviates from point like behavior which implies scaling violations. Again the scaling violations are relatively small effects over the range of data available, and are difficult to interpret[22].

There are some experimental directions which now seem more promising as probes of the $q\bar{q}$ and gluon-gluon force, and so are tests of the local $SU(3)_{color}$ gauge symmetry. One direction is the one we will discuss in these lectures, namely quarkonium spectroscopy. Others are gluonium spectroscopy[23], and gluon bremsstrahlung[24]. These last three processes are depicted graphically in figure 10.

In all the experiments we have mentioned, an important goal of the experiment is typically the determination of $\alpha_s(s)$; what is $\alpha_s(s)$? Each experimental situation can yield a somewhat different definition due to

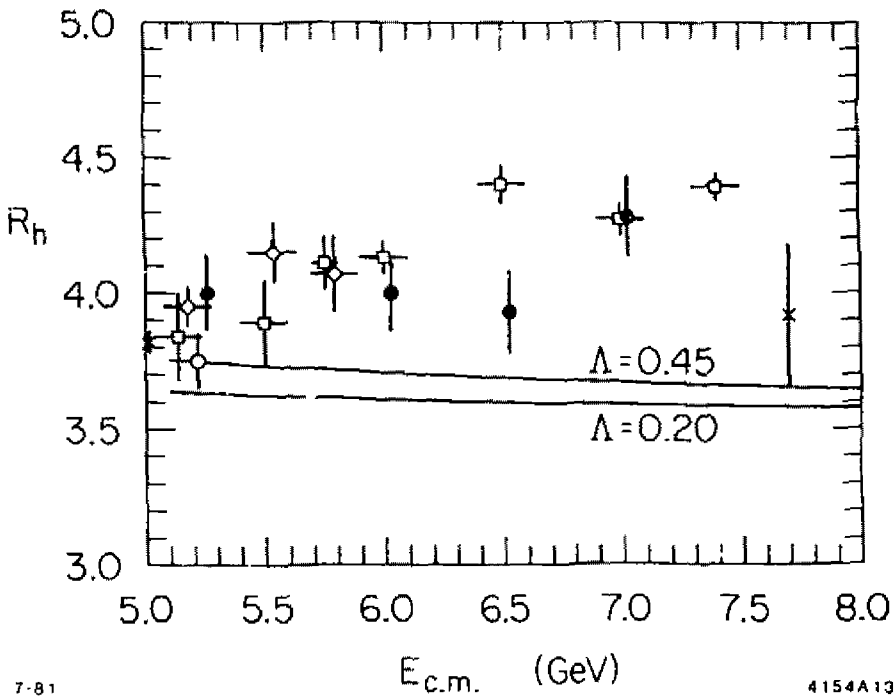

Figure 9. R_h from various experiments and comparison with QCD. σ_τ has been subtracted. The data are radiatively corrected. Only the statistical errors are shown, systematic errors vary between 6 and 19 percent[19]. ▣ MARK I, ◈ MARK II, ✖ PLUTO, ○ XTAL BALL(1979), ● XTAL BALL(1981). The QCD theory is shown as ▬ for $0.2<\Lambda<0.45$ and was obtained from Reference 21.

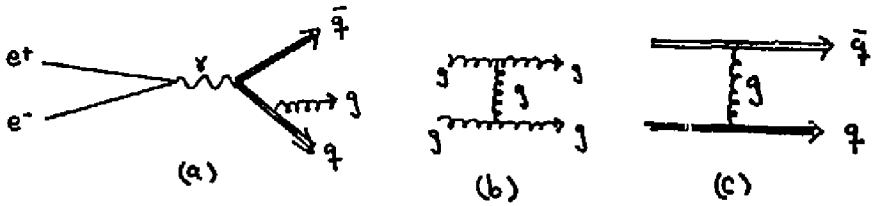

Figure 10. Promising directions for probing $SU(3)_{color}$ local gauge symmetry. a). Gluon Bremsstrahlung.
b). Gluon-Gluon Force (Gluonium).
c). Quarkonium ($q\bar{q}$ Force).

higher order effects. In the case of quarkonium, to lowest order, the color charge is given by,

$$Q^{ij}_{q} = \lambda^{ij}\sqrt{\alpha_s(s)} \qquad \text{(III-14)}$$

Where the λ^{ij} are the familiar $SU(3)_{color}$ matrices, and the $q\bar{q}$ interaction is[25],

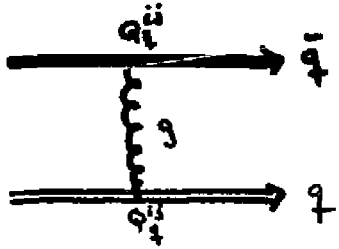

$$\rightarrow V(\hat{q}^2) = -(4/3)\alpha_s(\hat{q}^2)/\hat{q}^2 \qquad \text{(III-15)}$$

Where, $\hat{q}^2 = (\vec{q}_i - \vec{q}_j)^2$, is the three vector momentum transfer.

Note that for QED,

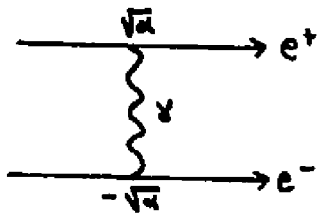

$$\rightarrow V(\hat{q}^2) = -\alpha/\hat{q}^2 \qquad \text{(III-16)}$$

Where in this case $\alpha \approx 1/137$.

Thus we obtain the important substitution rule[25] relating α_{qed} and α_s for single gluon exchange,

$$\alpha_{qed} \rightarrow (4/3)\alpha_s(\hat{q}^2) \quad . \qquad \text{(III-17)}$$

So combining equation (III-11), for $\alpha_s(s)$, with our interpretation of $\alpha_s(\vec{q}^2)$, given by (III-15), we find that the strength of the $q\bar{q}$ interaction is characterized by $\alpha_s(\vec{q}^2) \to 0$ as $\vec{q}^2/\Lambda^2 \to$ large, as is the case for heavy quarkonium states. This result is called asymptotic freedom (AF)[14]. Also, given that quarks are confined in hadrons, we must have $\alpha_s(\vec{q}^2) \gg 1$ for $\vec{q}^2 \leq$ (1 fermi)$^{-2}$; this feature of the theory is called infrared slavery (IS)[14].

Equations (III-15) and (III-16) look a lot alike, particularly when $\alpha_s(\vec{q}^2) \approx \alpha_{QED}$. This is the source of the analogy which led to the original ansatz[24] that charmonium with $s \approx 10 GeV^2 \gg$ (1 fermi)$^{-2}$ should have characteristics much like positronium. However, as figure 11 shows, $\alpha_s(10GeV^2) \approx 0.2 \gg 1/137$. Even at the Υ, $\alpha_s \approx 0.17$ and so the simple coulomb-like potential is only part of the story.

c). The charmonium model.

In 1974 Appelquist and Politzer[26] made the QED-QCD connection for $s \approx 10$ GeV^2 and suggested that $c\bar{c}$ bound states might exist in the region $3.0 < E_{cm} < 4.0$ GeV. However, what really started serious consideration that the $c\bar{c}$ system could have a non-relativistic bound state spectrum was the discovery of J/ψ and ψ' in 1974. (See figure 12.)

The case for a new charmed quark was clinched with the discovery of charmed mesons in 1976[30]. The masses of these mesons supported the idea that the charmed quark mass was about half the mass of the J/ψ. Thus the way was clear to take the non-relativistic charmonium model quite seriously.

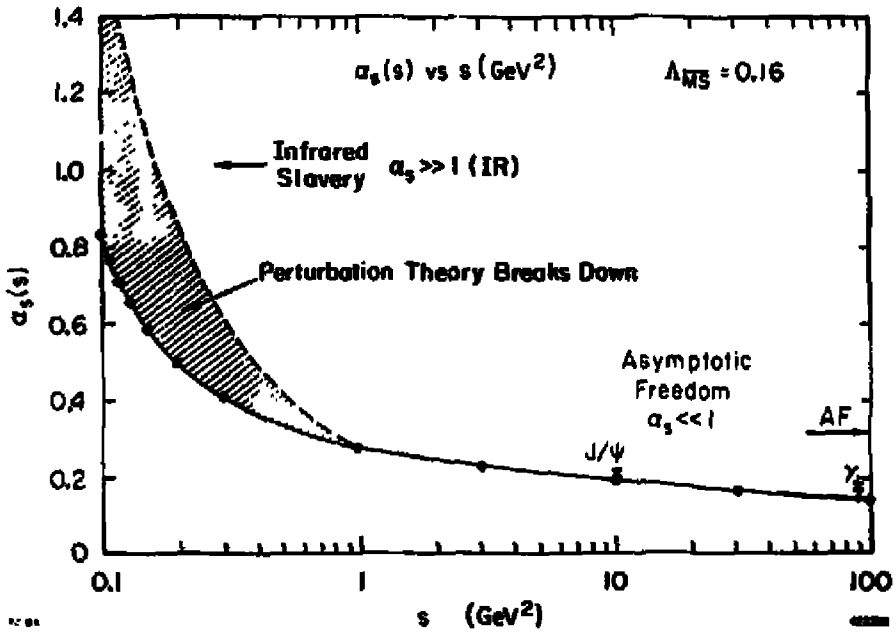

Figure 11. $\alpha_s(s)$ vs. s as calculated from (III-11) with $\Lambda_{\overline{MS}} = 0.16$ GeV. The measured values for α_s obtained by experiment at the J/ψ and Υ are also shown. PETRA experiments[24] have obtained $\alpha_s(900GeV^2) = 0.17 \pm 0.02 \pm 0.03$ by analyzing the gluon bremsstrahlung process shown in Figure 10, while the theory yields about 0.12 at s = 900 GeV.

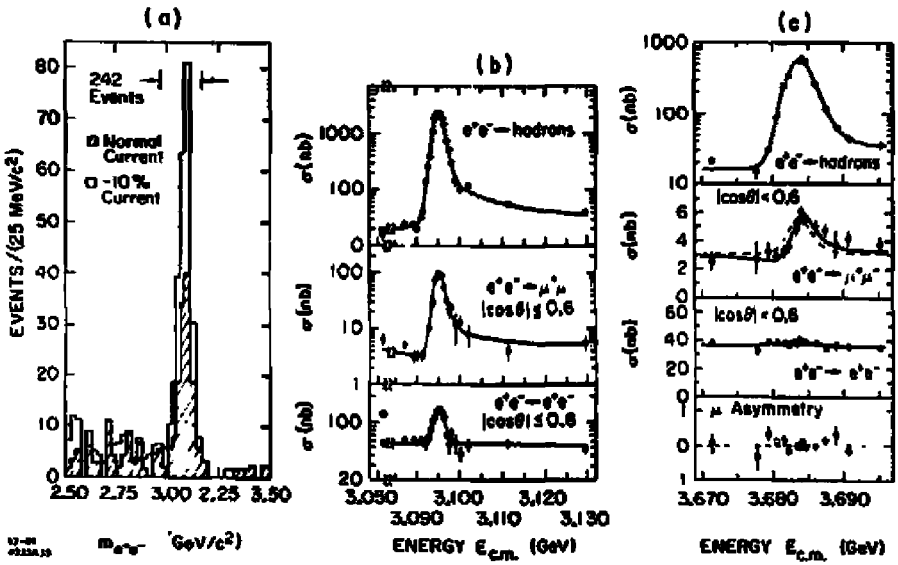

Figure 12. a). The Observation of the J at BNL[27]. The Figure shows the e^+e^- effective mass spectrum from the reaction pBe → e^+e^-X. b). The observation of the ψ at SLAC[29]. The Figure shows the Energy Dependence of the Cross Sections e^+e^- → hadrons, e^+e^- → $\mu^+\mu^-$ and e^+e^- → e^+e^- in the vicinity of the ψ. c). The Energy Dependence of the Cross Sections e^+e^- → hadrons, e^+e^- → $\mu^+\mu^-$, e^+e^- → e^+e^- and the Foward-Backward Asymmetry in μ pair production in the vicinity of the ψ'. This Figure is essentially from reference 29.

In order to explore the consequences of the non-relativistic $c\bar{c}$ bound state model we use the Schroedinger equation[16] (in contradiction to the experience with positronium where a relativistic formulation of the theory has been used). There are three aspects to the model which will be considered, and later compared to experiment:

- Calculation of energy levels and wavefunctions.
- Calculation of the widths of the states.
- Calculation of the photon transitions between states.

First we must find the masses of the states and their wavefunctions. To accomplish this a potential, V(r) is needed. Initially potentials were constructed which separately included AF and IS.

$$H\psi = E\psi, \text{ with initially} \qquad \text{(III-18)}$$

$$H = p^2/M_0 + V(r), \qquad \text{(III-19)}$$

$$V(r) = \kappa/r + r/a^2 \qquad \text{(III-20)}$$

Where the first term on the right of (III-20) is an attempt to include AF, and the second term approximates IS[16]. M_0 is the mass of the charmed quark. κ and a^2 are parameters. Agreement with experiment is spotty using (III-18) - (III-20) as we will discuss. However, in the last few years, more sophisticated potentials have been used which have been derived more closely from QCD. These newer potentials have had greater success.

To describe the quarkonium spectroscopy, the spin-orbit (l-s) and spin-spin (hf-s) potentials are also needed. These can be obtained from an "Instantaneous Bethe-Salpeter Kernal consisting of vector and scalar interaction terms related to single gluon exchange with renormalization improvement."[16a] Given by,

$$V_{coul}(\vec{q}^2)\gamma_c^\mu\gamma_{\bar{c}\mu} + V_v(\vec{q}^2)\Gamma_c^\mu(q)\Gamma_{\bar{c}\mu}(q) + V_s(\vec{q}^2)1_c1_{\bar{c}} \qquad \text{(III-21)}$$

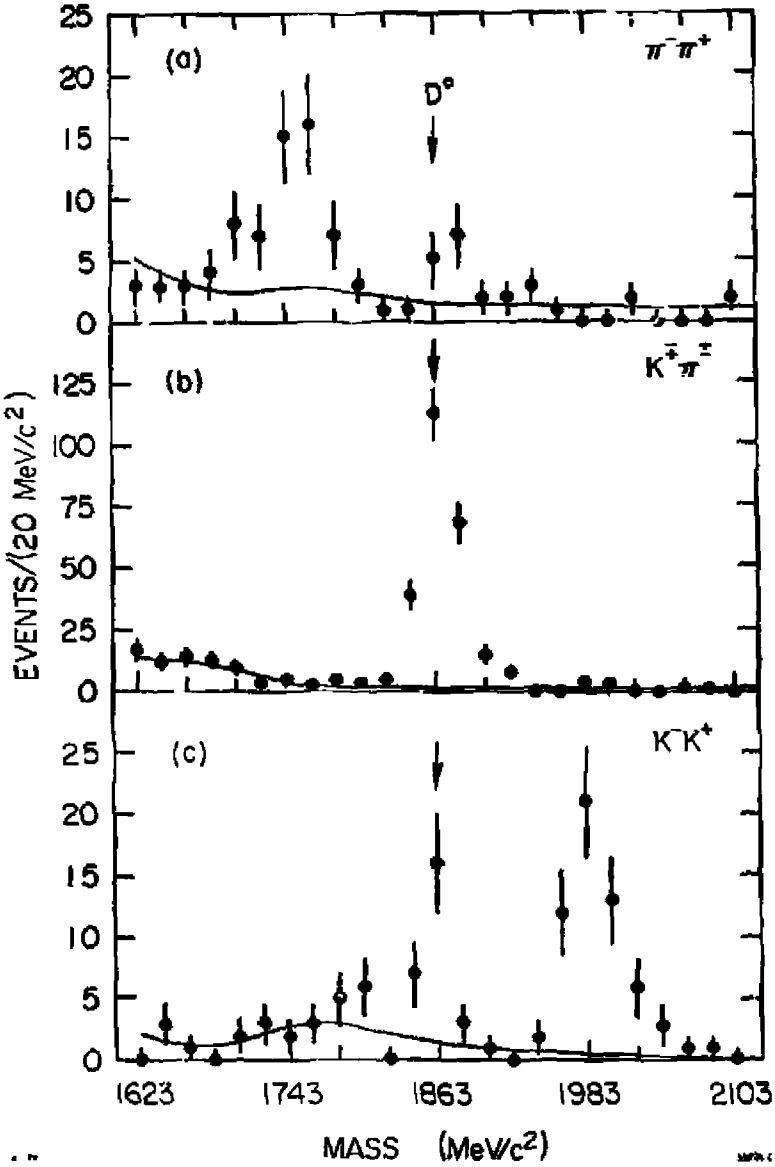

Figure 13. The proof of charm. Invariant mass of two particle combinations with momenta within 30 MeV/c of the expected D^0 momentum[30].
a). $\pi^+\pi^-$, b). $K^\pm\pi^\mp$, c). K^-K^+.

I_c ($I_{\bar{q}}$) is the unit matrix in Dirac space, q is the four momentum of the gluon,

$$\Gamma_\mu(q) = \gamma_\mu - (i\lambda/2M_c)\sigma_{\mu\nu}\, q^\nu, \qquad \text{(III-22)}$$

where, $\sigma_{\mu\nu} = (1/2i)[\gamma_\mu,\gamma_\nu]$, λ is the anomalous color magnet moment of the quark. Note that $V_v(\vec{q}^2)$ is a vector like potential while $V_s(\vec{q}^2)$ is a scalar potential.

Taking the spin-independent, non relativistic limit of (III-21) we find that the potential is, in configuration space,

$$V_0 = \kappa/r + r/a^2 = V_{coul} + (V_v(r) + V_s(r)) \qquad \text{(III-23)}$$

It is usually assumed that,

$$V_v(r) = \eta r/a^2\ ,\ V_s(r) = (1-\eta)r/a^2, \qquad \text{(III-24)}$$

The actual spin-dependent potential is obtained through analogy to QED in the reduction of the Bethe-Salpeter Kernal into the Breit Interaction[16a],

$$\begin{aligned} V_{spin}(\vec{r}) = {} & (1/2M_c^2)[4\kappa/r^3 + 4(1+\lambda)(1/r)dV_v/dr - (1/r)dV_0/dr]\vec{L}\cdot\vec{S} \\ & +2/3M_c^2[4\pi\kappa\delta(\vec{r}) + (1+\lambda)^2\nabla^2 V_v(r)]\vec{S}_c\cdot\vec{S}_{\bar{c}} \\ & +1/3M_c^2[3\kappa/r^3 + (1/r)dV_v/dr - d^2V_v/dr^2]S_{c\bar{c}} \end{aligned} \qquad \text{(III-25)}$$

where, $\vec{S} = (\vec{S}_c + \vec{S}_{\bar{c}})$,

$$S_{c\bar{c}} = 3(\vec{S}_c\cdot\hat{r})(\vec{S}_{\bar{c}}\cdot\hat{r}) - \vec{S}_c\cdot\vec{S}_{\bar{c}},\ \hat{r} = \vec{r}/r, \qquad \text{(III-26)}$$

and $\vec{S}_c(\vec{S}_{\bar{c}})$ is the spin operator for the c($\bar{c}$). The $-(1/r)\,dV_0/dr$ part of the first term arises from the Thomas precession effect.

For the potential of equations (III-23, III-24),

$$\begin{aligned} V_{spin}(\vec{r}) = {} & 1/2M_c^2[3\kappa/r^3 + 1/ra^2\,(\eta(3+4\lambda) - (1-\eta))]\vec{L}\cdot\vec{S} \\ & +2/3M_c^2[4\pi\kappa\delta(\vec{r}) + 2\eta/ra^2(1+\lambda)^2]\vec{S}_c\cdot\vec{S}_{\bar{c}} \\ & +1/3M_c^2[3\kappa/r^3 + \eta/ra^2\,(1+\lambda)^2]S_{c\bar{c}} \end{aligned} \qquad \text{(III-27)}$$

For the simplest case, $\lambda = 0$, $\eta = 0$, and we find,

$$V_{spin}(\vec{r}) = 1/2M_c^2[3\kappa/r^3 - 1/ra^2]\vec{L}\cdot\vec{S} \quad [1]$$

$$+2/3M_c^2[4\pi\kappa\delta(\vec{r})]\vec{S}_c\cdot\vec{S}_{\bar{c}} \quad [2]$$

$$+1/3M_c^2[3\kappa/r^3]S_{c\bar{c}} \quad [3] \qquad \text{(III-28)}$$

Terms [1] and [3] contribute to the spin-orbit f-s, with,

j	$\langle\vec{L}\cdot\vec{S}\rangle$	$\langle\vec{S}_{c\bar{c}}\rangle$
$\ell+1$	ℓ	$-2\ell/(2\ell+3)$
ℓ	-1	2
$\ell-1$	$-(\ell+1)$	$-2(\ell+1)/(2\ell-1)$

Table 5. Spin-orbit f-s matrix elements

Term [2] contributes to the hf-s only.

$$\langle\vec{S}_c\cdot\vec{S}_{\bar{c}}\rangle = -3/4(\text{singlet}),\ 1/4(\text{triplet}) \qquad \text{(III-29)}$$

Then

$$H = P^2/M_c + V_0 + V_{spin} \qquad \text{(III-30)}$$

Now that the masses and wave functions are known (in principle) we also want to calculate the widths of the states. To accomplish this we use QED positronium results plus the substitution rules $\alpha_{qed}^n \rightarrow (\text{color factor})\alpha_s^n$. Thus using equation (III-6) and $\alpha_{qed}^2 \rightarrow (2/3)\alpha_s^2$ (see reference 16b), we obtain,

$$\Gamma(\eta_c \rightarrow gg(\rightarrow\text{hadrons})) = (8/3)\ \alpha_s^2|R(0)|^2/M^2_{\eta c} \qquad \text{(III-31)}$$

Where we define $|R(0)|^2 = |\Psi(0)|^2 4\pi$, the radial part of the wavefunction at the origin. Using equation (III-7) and $\alpha_{qed}^3 \rightarrow (5/18)\alpha_s^3$ (see reference 16b), we obtain,

$$\Gamma(J/\Psi \rightarrow ggg) = (40(\pi^2-9)/81\pi)\alpha_s^3|R(0)|^2/M^2_{\Psi} \qquad \text{(III-32)}$$

Also, (see reference 25),

$$\Gamma(J/\psi \to \ell^+\ell^-) = 4\alpha^2 Q_c^2/M^2_\psi |R(0)|^2, \qquad \text{(III-33)}$$

Finally, we would like to calculate the γ transition rates between charmonium states. We use old fashioned perturbation theory, and assume that relativity is not important.

Electric dipole, E_1, transitions, e.g., $2^3S_1 \to \gamma\ 2^3P_1 \to \gamma\ \gamma\ 1^3S_1$.

$$\Gamma(S \langle - \rangle P) = 4/9[(2j_f+1)/(2j_i+1)]Q_c^2\alpha|E_{if}|^2\omega^3, \qquad \text{(III-34)}$$

where ω is the γ-energy, $j_i(j_f)$ the total angular momentum of the initial (final) state, and,

$$E_{if} = \int_0^\infty r^2 dr[\Psi_i(r)\Psi_f(r)r] \qquad \text{(III-35)}$$

Magnetic dipole, M_1, transitions, (allowed M1), e.g., $1^3S_1 \to \gamma\ 1^1S_0$.

$$\Gamma(^3S_1 \langle - \rangle\ ^1S_1) = 16/3\ (2j_f+1)(Q_c/2M_c)\alpha|M_{if}|^2\omega^3 \qquad \text{(III-36)}$$

where,

$$M_{if} = \int_0^\infty r^2 dr[\Psi_i(r)\Psi_f(r)j_0(\omega r/2)] \qquad \text{(III-37)}$$

Note:

$M_{if} \propto 1$ since $\Psi_i = \Psi_f$ and $j_0(\omega r/2 \ll 1) \propto 1$.

M_1 transitions, (hindered), e.g., $2^3S_1 \to \gamma\ 1^1S_0$. Neglecting relativistic effects and $2^3S_1 - 3^3D_1$ mixing,

$$\Gamma(n^3S_1 \to (n-1)^1S_0) \propto 0, \qquad \text{(III-38)}$$

$$\text{since, } M_{ij} \propto -\int_0^\infty r^2 dr(\omega^2/24)[\Psi_i(r)\Psi_j(r)r^2] << 1. \qquad \text{(III-39)}$$

d) Comparison of the charmonium model to experiment.

Using the theoretical development of the last section, we can now make some detailed comparisons with experiments. κ, a^2 and M_c are adjustable parameters so three constraints are needed to fix these constants. Also, as we move from the $c\bar{c}$ to $b\bar{b}$ quark systems we expect $M_c \rightarrow M_b$, $\kappa_b < \kappa_c$, (AF), and $a_c^2 \propto a_b^2$. Our comparison of theory to experiment will dicuss:

- The masses of the charmonium and bottomonium systems.
- $n^{2s+1}L_j^{PC}$ Classification of observed states.
- The hadronic and leptonic width of states.
- The rates of γ transitions between states, and the multipolarity of the transitions.

Mass of states:

A number of techniques are available to establish the onium state masses. First, the storage ring energy, which is typically known to 0.1%, can be used to measure the $n^3L_1^{--}$ masses with high precision. An example of such a measurement is shown in figures 12 b), c). Second, the hadronic decays of the states not accessible to direct production can be used to measure their masses with a somewhat limited accuracy of about 1% -2%. The limit in accuracy is due to the limit in momentum and angular resolution of most detectors presently operating. An example of such a measurement is shown in figure 13 for D^0 mesons. Finally, the photon transitions between the states can be used inclusively, or exclusively in fits using hadronic

information, to determine the masses of the bound n^3P_j's, and n^1S_0's to high accuracy once the n^3S_1's masses are known. This is because the γ energies for the transitions are typically less than 10% of the mass of the states. In the case of inclusive photon measurements, as shown in figure 14, accuracies of about 0.2% - 0.4% are obtainable. For exclusive fits somewhat more accurate results can be achieved, depending on the detector.

Fine Structure and Hyper fine Structure:

A number of attempts have been made to fit the f-s and, until recently, to predict the hf-s. Though the models have had some qualitative success, none has been able to accurately predict the f-s, and hf-s. Most models have had a lot of variability in their predictions due to the large number of parameters (5 or 6) available to them. For example, before the X(2830)[34] was shown not to exist,[35] it was taken as the η_c. The large hf-s of $\approx$ 260 MeV presented by this assignment was eventually fit by most models. Only a few calculations denied this possibility[36], and these were estimated to be good to only $\pm$ 30% of the transition γ energy. Table 6 shows recent experimental values for the charmonium f-s and hf-s splittings as well as two sets of predictions of the type discussed in the previous theory section[16a]. For both sets of predictions λ, the quark anomalous moment, is taken as 0 since little evidence exists for a non-zero value.

Theory 1: κ=0.2, $1/a^2$=0.19, M_c=1.6 Gev, η=1, λ=0.

Theory 2: κ=0.8, $1/a^2$=0.18, M_c=1.6 Gev, η=0, λ=0.

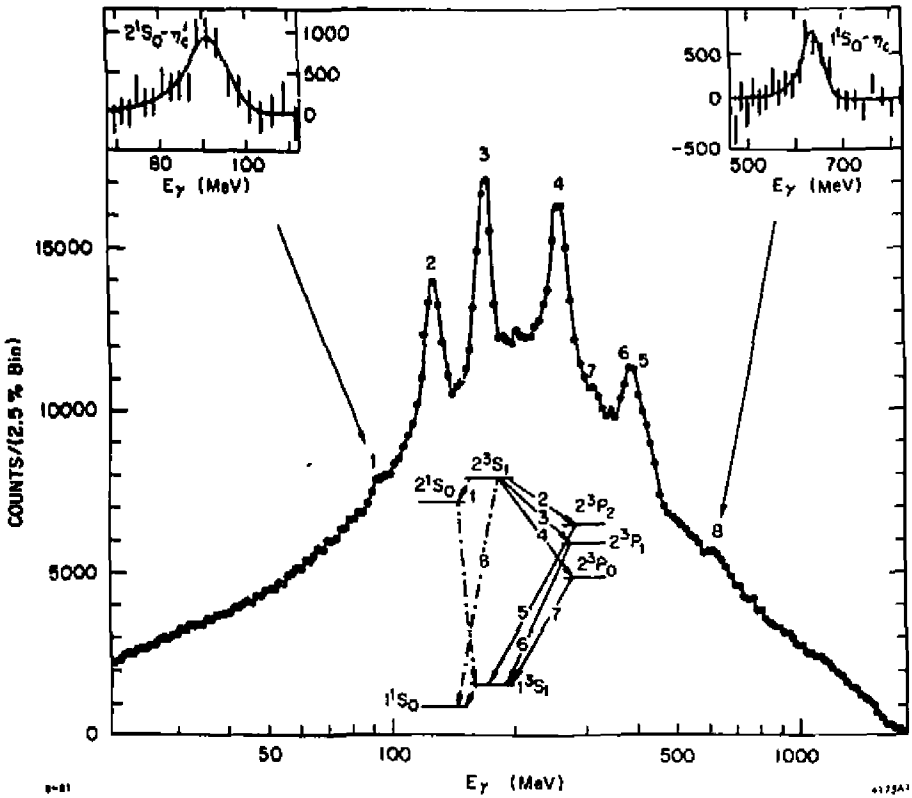

Figure 14. The inclusive γ spectrum obtained from = 1.7M hadronic ψ' decays in the cyrstal ball detector. The lower insert shows the bound state charmonium level diagram, except for the 2^1P_1[+-] which can only be seen as a γ transition from one of the other P states (if the energies are right) and so should be very weak. All the transitions shown in the level diagram appear as lines in the spectrum. The weaker transitions to the η_c[31] and η_c'[32] are shown in blowups of the inclusive γ spectrum in the region of the respective lines. The left upper corner contains the η_c' spectrum ,the right upper corner the η_c spectrum. For details of the measurement, including a careful discussion of this new η_c' candidate, see reference 33.

Mass Difference	Experiment	Theory 1, Theory 2
1) $M_{\psi} - M_{\eta c}$ (hf-s)	111 ± 5 MeV[33]	70, 95 MeV
2) $M_{x2} - M_{x1}$ (f-s)	45.5 ±0.70[30]	87, input
3) $M_{x1} - M_{x0}$ (f-s)	95.5 ±0.9[30]	63, 80
4) $M_{\psi'} - M_{\eta c'}$ (hf-s)	91 ±5[32]	58, --

Table 6. Comparison of experimental f-s and hf-s to two charmonium models.[16] Note: $\Delta M_{f\text{-}s} = 2)/3) = 0.48 \pm 0.01)_{exp}$, while, $\Delta M_{f\text{-}s} = 1.38)_{theory1}, = 0.57)_{theory2}$. Thus theory 2 which has V_s dominant, which is equivalent to a large Thomas precession term, $-1/r a^2\ (1-\eta)\vec{L}\cdot\vec{S}/2M_c^2$, in first line of (III-27)), is able to reproduce the observed $\Delta M_{f\text{-}s}$ by canceling off a large part of the $\vec{L}\cdot\vec{S}$ term. The tensor part of the f-s interaction then dominates.

Classification, $n^{2s+1}\ell_j^{PC}$:

A number of pieces of information must be combined to determine the j^{PC} of a state. The $n^3S_1^{--}$ states are relatively easy to identify since they are produced directly in e^+e^- annihilation. The observation of an interference with other annihilation channels, e.g., see figure 12 c), unambiguously assigns a state's j^{PC} as 1^{--}. The $n^3P_j^{++}$ states, called the x states in the charmonium system, pose a more difficult problem. Two types of information have been used to assign these states.

An analysis of the cascade process,

$$\psi' \to \gamma\, x \to \gamma\,\gamma\, J/\psi \to \gamma\,\gamma\, \ell^+\,\ell^- \qquad \text{(III-40)}$$

yields the j of the state only, not P (we know C = + because of the first decay of (III-40)). An angular correlation analysis[37] is done which fits

the γ and final state lepton angles to a probability distribution.

$$W_j(\cos\theta',\phi',\cos\theta_{\gamma\gamma},\cos\theta,\phi,\vec{p}); \qquad \text{(III-41)}$$

e.g., for j=0,

$$W_0 = (1 + \cos^2\theta')(1 + \cos^2\theta) \text{ (dipole only for j=0)} \qquad \text{(III-42)}$$

where the angles are defined in figure 15, and $\vec{p}$ indicates the multipole content of W_j. For a spin j χ state there are 2j+1 multipole amplitudes for the transition $\psi' \to \gamma \chi_j$, and another 2j+1 amplitudes for $\chi_j \to \gamma J/\psi$. These are usually called dipole, quadrupole, octupole, ..., amplitudes and in lowest order are electric dipole (E1) for χ_j parity + or magnetic dipole (M1) for χ_j parity -. The angular correlation analysis alone cannot determine whether electric or magnetic amplitudes are operative, i.e., as mentioned previously, the parity of the χ_j state is not determined in this analysis. In the non-relativistic charmonium model, lowest order is assumed to be dominant. Thus, only the dipole contribution is considered, c.f. equations (III-34) and (III-36). This is an assumption which has been checked experimentally, as will be shown later. The results shown here are a partial summary of those presented in reference 38.

Before considering the full spin analysis, much can be learned (and historically was) by examining the hadronic decay modes of the various χ states, and by analyzing the distribution of the first γ, in $\cos\theta'$. This knowledge of the initially emitted γ in the cascade is obtained, along with the hadronic decay information, from a common 1-C kinematic fit in the case of the Mark I[29] and Mark II[39] detectors. Similar information is obtained from the Crystal Ball detector by observing all γ decays of the χ states, e.g., $\chi_0 \to \pi^0\pi^0$, a 1-C fit in this detector. The $\chi(3.55)$ and $\chi(3.41)$ both decay into two pseudoscalars, $\pi\pi$ or KK, while the $\chi(3.51)$ does not[29,39].

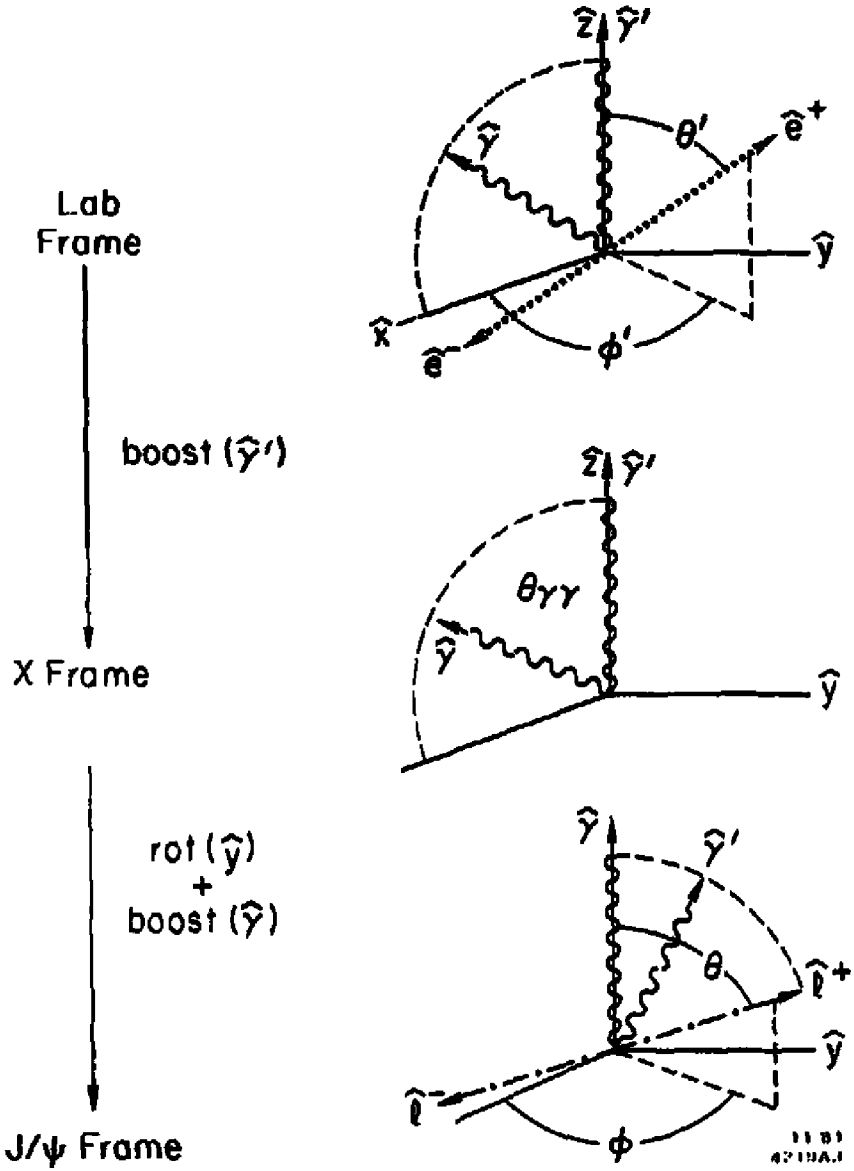

Figure 15. Vectors, angles and frames describing the cascade reaction

This is illustrated using recent Crystal Ball data in figure 16. Thus the $\chi(3.55)$ and $\chi(3.41)$ must have $J^{PC} = 0^{++}, 2^{++}\ldots$, using P and C conservation in the decays.

The $\chi(3.51)$ is observed[39] to decay into $K\bar{K}\pi^0$ (three pseudoscalars) and thus 0^+ is not possible for this state. The absence of a prominent decay into 2γ for such a narrow state (it is narrower than the $\chi(3.55)$ as we shall discuss), strongly indicates, though does not prove, a spin-parity assignment 1^+ or 1^-. (A massive spin 1 object can't decay into two massless spin 1 objects, or Yang's theorem.)

Figure 17 shows the projection on $\cos\theta'$ of the data of references 38(crystal ball), 29(SLAC-LBL). There is a good indication for a $J = 0$ assignment for the $\chi(3.41)$; the $\chi(3.51)$ is clearly not $J = 0$, as we already know. For a conclusive J assignment of $\chi(3.55)$ and $\chi(3.51)$ the full correlation analysis is needed. Note that the rate for (III-40) for $\chi(3.41)$ is very small and so a full analysis cannot be done to determine J for this state with existing data which comes from $\approx 1.7M$ ψ' decays. The likely assignment of 0^{++} for $\chi(3.41)$ is thus commonly accepted.

A maximum likelihood fit over all angles and multipole coefficients establishes the spin assignment with certainty when sufficient data are available as is the case for data obtained by the Crystal Ball[38] for $\chi(3.55)$ and $\chi(3.51)$. These fits favor $\chi(3.55)$ having $J=2$ over $J=1,0$ by many standard deviations, also $\chi(3.51)$ has $J=1$ by a few standard deviations (≈ 4) over $J=2,0$.

We thus conclude that,

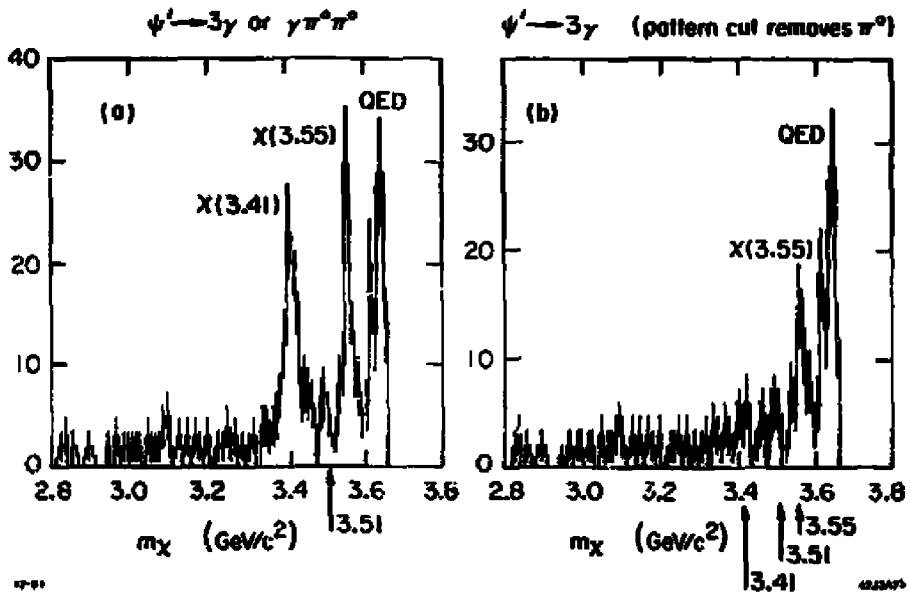

Figure 16. a) $\psi' \to 3\gamma$ or $\gamma\pi^0\pi^0$ as observed by the Crystal Ball Detector. $\chi(3.41)$ and $\chi(3.55)$ show prominent signals while, $\chi_1(3.51)$ does not. b) $\psi' \to 3\gamma$ (after π^0 removal). A strong signal still appears for $\chi_2(3.55)$ (though smaller than in figure 16a), while none appears for $\chi_0(3.41)$. Thus we conclude, $\chi(3.41)$ and $\chi(3.55)$ both decay to $\pi^0\pi^0$, while $\chi(3.51)$ does not. Also, $\chi(3.55)$ has an observable decay to $\gamma\gamma$. Note that the last peak on the right in both parts of the figure is just the QED process, $e^+e^- \to 3\gamma$.

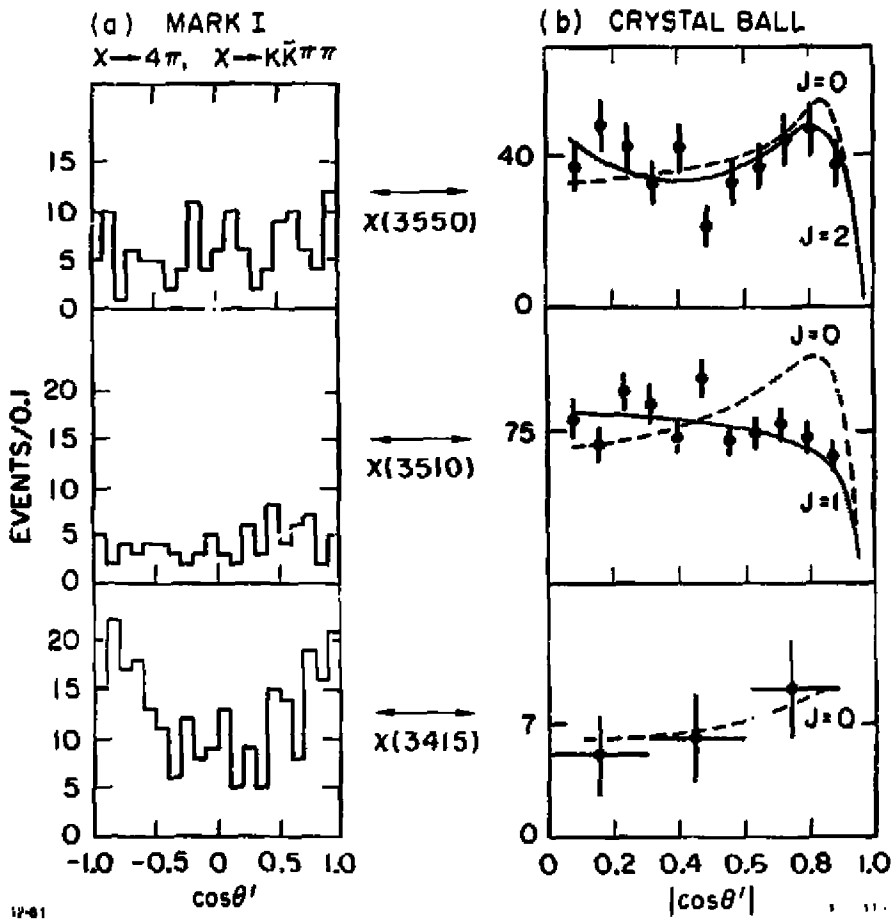

Figure 17. a) Data from the Mark I [29] detector for $\psi' \to \gamma\chi$, $\chi \to 2\pi^+2\pi^-$ or $K^+K^-\pi^+\pi^-$. The angular distribution n $\cos\theta'$ of the transition γ is shown for each χ state. $\chi(3.41)$ is consistent with a $1 + \cos^2\theta'$ distribution while the other χ states are not. b) Data from the Crystal Ball detector [28] for $\psi' \to \gamma\chi \to \gamma\gamma J/\psi \to \gamma\gamma\ell^+\ell^-$. Again the angular distribution in $\cos\theta'$ of the first γ transition is shown for each χ state. Also, Monte Carlo results for various spin assignments are shown. $\chi(3.41)$ is consistent with a $1 + \cos^2\theta'$ distribution, (j = 0). Based on a) and b) plus the arguments in the text, a 0^{++} assignment for $\chi_0(3.41)$ is most likely, and is commonly accepted.

$$2^3P_J^{++} = \chi(3.55) = \chi_2$$

$$2^3P_1^{++} = \chi(3.51) = \chi_1 \text{(parity not directly measured)} \qquad \text{(III-43)}$$

$$2^3P_0^{++} = \chi(3.41) = \chi_0$$

just as one expects from the charmonium model. The $\eta_c(2980)$ and $\eta_c'(3592)$ have $C=+$; however, the determination of J^P for these states needs further experiments (transition γ cosθ^* distribution, $\gamma\gamma$ and hadronic decays spin analysis).

Widths of States. The leptonic branching ratio of the J/ψ can be used to estimate $\alpha_s(M_\psi^2)$. To form this branching ratio we use (III-32) and (III-33) as well as:

$$\Gamma(J/\psi \to \gamma gg) \quad 32/9\pi\ (\pi^2-9)\alpha_s^3\alpha Q_c^2 |R(0)|^2/M_\psi^2 \qquad \text{(III-44)}$$

we then find, in lowest order,

$$Br(J/\psi \to e^+e^-) = Br(J/\psi \to \mu^+\mu^-)$$

$$= \frac{\Gamma(J/\psi \to e^+e^-)}{\Gamma(J/\psi \to ggg) + 2\Gamma(J/\psi \to e^+e^-) + \Gamma(J/\psi \to \gamma gg)} \qquad \text{(III-45)}$$

or,

$$Br(J/\psi \to e^+e^-) = \frac{\alpha^2 Q_e^2}{10(\pi^2-9)/81\pi\ \alpha_s^3 + 2\alpha^2 Q_c^2 + 8/9\pi\ (\pi^2-9)\alpha_s^3\alpha Q_c^2} \qquad \text{(III-46)}$$

Numerically with $Q_c = 2/3$,

$$Br(J/\psi \to e^+e^-) = \frac{2.366 \times 10^{-5}}{3.417\times10^{-2}\ \alpha_s^3 + 4.736\times10^{-5} + 7.983\times10^{-6}\alpha_s^2} \qquad \text{(III-47)}$$

which is a cubic equation for α_s.

Experimentally,[17]

$$Br_{exp}(J/\psi \to e^+e^-) = 7.21\times10^{-2} \qquad \text{(III-48)}$$

solving (III-47) using (III-48) we find,

$$\alpha_s(M_\psi^2) = .197 \pm 0.010 \qquad \text{(III-49)}$$

where this result is for first order QCD, i.e., $\alpha_s^0(M_\psi^2)$ has actually been determined.

A recent evaluation[51] using the J/ψ - η_c mass difference as input yields $\Lambda_{\overline{MS}} = 0.16 \pm 0.02 \pm 0.07$, which implies to second order in QCD ($\overline{MS}$ renormalization scheme),

$$\alpha_s(M_\psi^2) = 0.18 \qquad \text{(III-50)}$$

or to first order QCD,

$$\alpha^0_s(M_\psi^2) = 0.24. \qquad \text{(III-51)}$$

For our purposes here, we will use,

$$\alpha_s(M_\psi^2) = 0.2 \pm 0.02. \qquad \text{(III-52)}$$

Using equations (III-31) and (III-32),

$$\Gamma(J/\psi \to 3g)/\Gamma(\eta_c \to 2g) = \alpha_s(M_\psi^2)[5(\pi^2-9)/27\pi]$$

$$= (1.0 \pm 0.1) \times 10^{-2} \qquad \text{(III-53)}$$

By using the experimental value [17]

$$\Gamma_{tot}(J/\psi) = 63 \pm 9 \text{ KeV}, \qquad \text{(III-54)}$$

and removing the partial widths, $\Gamma(J/\psi \to \ell^+\ell^-)$ and $\Gamma(J/\psi \to \gamma gg)$ (c.f. (III-33) and (III-44)) which have the values about 5.5 KeV and 5.3 KeV respectively, we find,

$$\Gamma_{th}(\eta_c \to gg(\text{hadrons})) = 4.7 \pm 1.2 \text{ MeV}. \qquad \text{(III-55)}$$

Using the inclusive γ spectrum from the J/ψ the Crystal Ball Collaboration has obtained [33],

$$\Gamma_{exp}(\eta_c \to \text{hadrons}) = 12.4 \pm 4.6 \text{ MeV}. \qquad \text{(III-56)}$$

Thus,

$$\Gamma_{th}/\Gamma_{exp}(\eta_c \to \text{hadrons}) = 0.38 \pm 0.17, \qquad \text{(III-57)}$$

where the error in the ratio is obtained from a Gaussian combination of the errors in (III-55) and (III-56). Depending on one's standards this is good

or poor agreement. After all, a first order theory is being used, and two quantities are being compared which are a factor of 100 different. Thus, obtaining agreement to a factor of 2-3 is somewhat gratifying. 1st order QCD also gives the χ state widths in terms of the first derivative of R(r) at the origin[16], i.e., $|R'(0)|^2$; For example

$$\Gamma(2^3P_2 \to \text{hadrons}) = 128/5\ \alpha_s^2\ |R'(0)|^2/M_{\chi 2}^4 \qquad \text{(III-58)}$$

and,

$$\Gamma(2^3P_0 \to \text{hadrons}) = 96\alpha_s^2|R'(0)|^2/M_{\chi 0}^4\ . \qquad \text{(III-59)}$$

Thus the ratio is a simple quantity,

$$\Gamma(2^3P_2 \to \text{hadrons})/\Gamma(2^3P_0 \to \text{hadrons}) = 4M_{\chi 0}^4/(15\ M_{\chi 2}^4) = 0.23\ . \qquad \text{(III-60)}$$

Using a combination of Crystal Ball results from the inclusive γ spectrum from the ψ′ [33] and cascade decays from the ψ′ to the J/ψ[38], the hadronic widths of the χ_0 and χ_2 states can be determined. Figure 18 shows the results obtained for the widths of the states from the cascade decays. Averaging the results from references 38 and 33 for the χ_2 width we find,

$$\Gamma_{exp}\ (\chi_2) = 3 \pm 1\ \text{MeV}. \qquad \text{(III-61)}$$

Also,[33]

$$\Gamma(\chi_2 \to \gamma J/\psi) = 330 \pm 170\ \text{KeV} \qquad \text{(III-62)}$$

and so, subtracting (III-62) from (III-61),

$$\Gamma(\chi_2 \to \text{hadrons}) = 2.7 \pm 1\ \text{MeV}. \qquad \text{(III-63)}$$

From the inclusive γ spectrum from the ψ′[33] ($\Gamma(\chi_0 \to \gamma J/\psi)$ is negligible),

$$\Gamma(\chi_0 \to \text{hadrons}) = 16 \pm 4\ \text{MeV} \qquad \text{(III-64)}$$

and thus we find,

$$\Gamma_{exp}(2^3P_2 \to \text{hadrons})/\Gamma_{exp}(2^3P_0 \to \text{hadrons}) = 0.17 \pm 0.08 \qquad \text{(III-65)}$$

or less than 1σ below the theoretical ratio (III-60). We thus again find

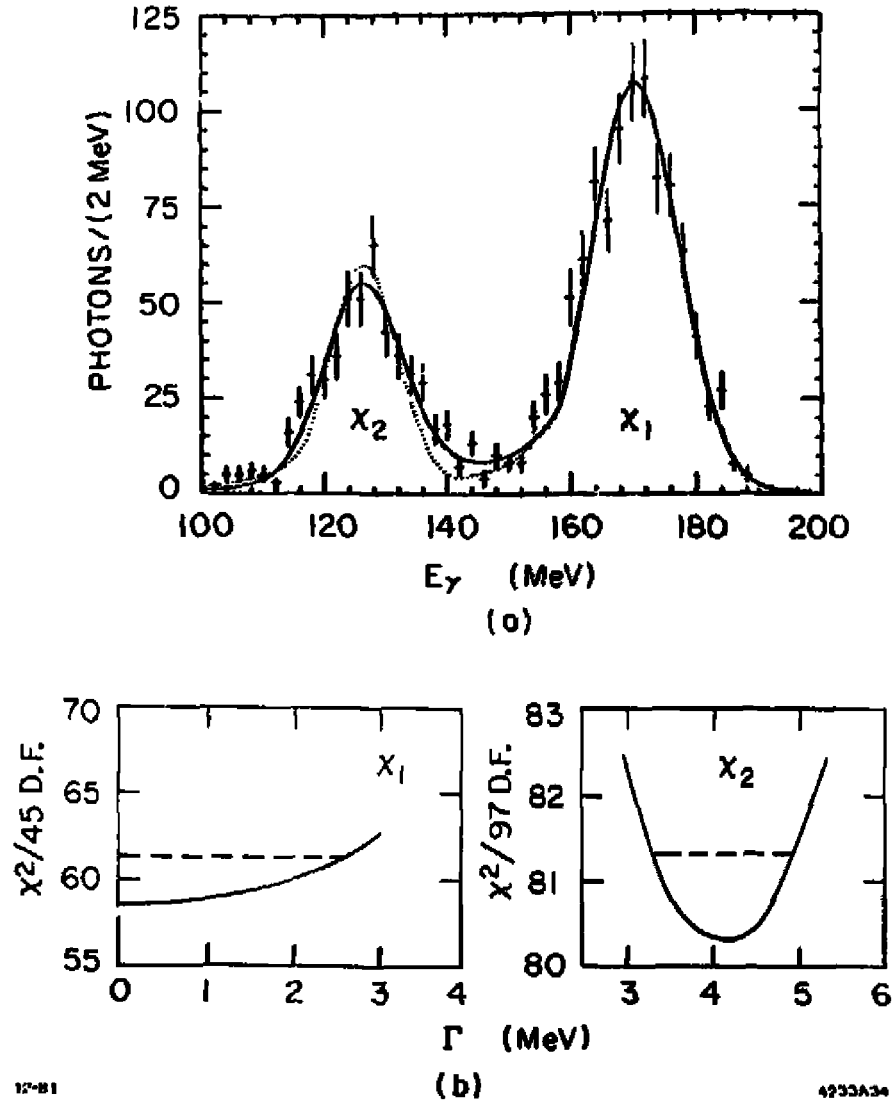

Figure 18. a) The spectrum of the first photon in the cascade $\psi' \to \gamma\chi \to \gamma\gamma J/\psi(\ell^+\ell^-)$ from the Crystal Ball Detector [38]. The spectrum is fitted by a convolution of the NaI line shape for the detector and a Breit-Wigner line shape. The dotted line is the NaI line shape. The solid line is the full fit. b) The confidence levels as a function of the Breit-Wigner full width, Γ, for χ_1 and χ_2. The horizontal dotted lines show the 90% C.L.), and the $\pm 1\sigma$ error limits for χ_2 (4.1 ± 0.9 MeV). The width measurement is clearly a tricky one

qualitative, though not convincing quantitative agreement between the first order theory and experiment. The absolute values of the widths are much worse; the $R'(0)$ obtained from an early charmonium model[16a], yields,

$\Gamma(2^3P_{0,1,2} \rightarrow \text{hadrons}) = 2$ MeV, 0.1 MeV, 0.5 MeV.

Rate and Multipolarity of χ Transitions.

To compare the charmonium model γ transitions rate predictions to experiment, we must first be sure that the model applies in principle. We have already checked aspects of the model in the previous sections. However, the non-relativistic approximation also demands dipole dominance for the γ transition matrix elements, i.e., that equations (III-34) - (III-39) apply. That the dipole matrix elements dominate the radiative transitions has been checked using the cascade process (III- 40). As described earlier, the j^{PC} of the χ states has been determined by using the cascade process and other inputs. In reference 38 fits of the form (III-41) were made to the cascade data for χ_1 and χ_2; dipole and quadrupole amplitudes were included in the fits. Figure 19 shows the results from the fitting process, and dipole amplitudes are shown to dominate.

Note that the radiative transition matrix elements measures the wave function at relatively large distance.

From the γ cascade analysis we compare $\Gamma(2^3S_1 \rightarrow \gamma 2^3P_j)$-$\Gamma(2^3P_j \rightarrow \gamma 1^3S_1)$ to the coupled channel Cornell Model (CCM)[42].

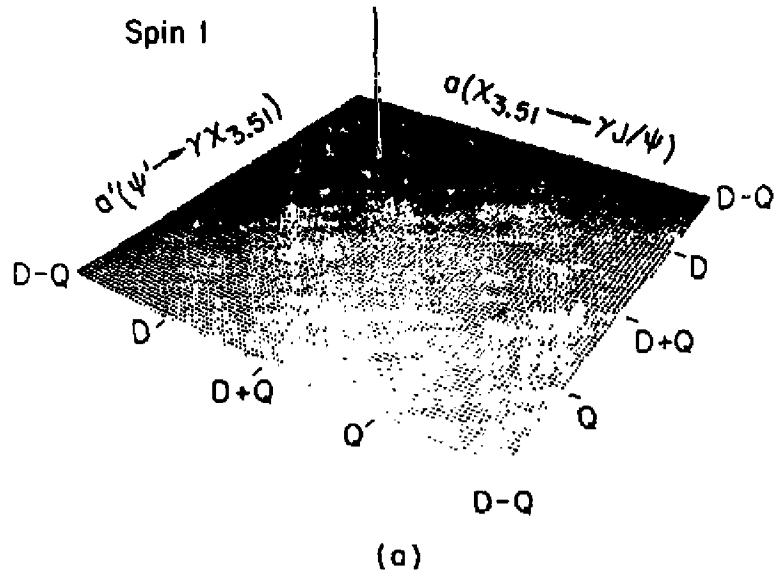

(a)

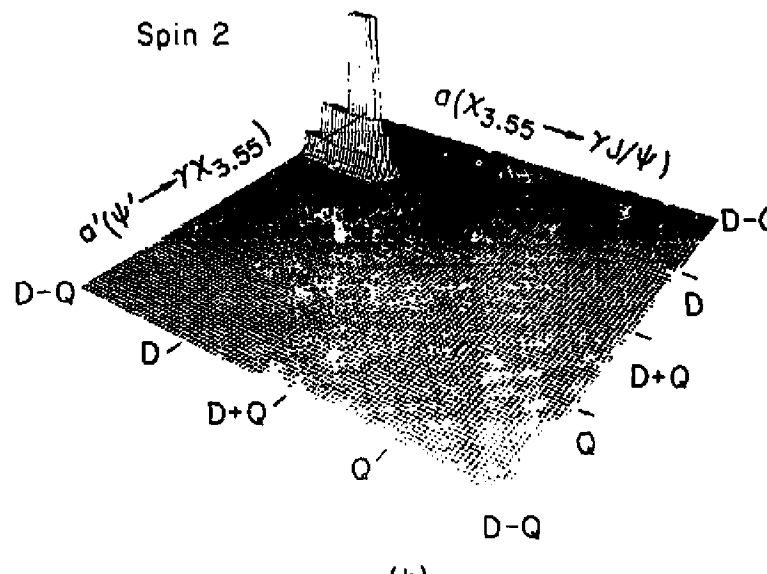

(b)

11-81 4216B16

Figure 19. The multipolarity content of the transitions for a) χ_1, and b) χ_2. The result is shown in terms of a likelihood function plotted as a function of D(dipole) and Q(quadrupole) amplitude content for $\psi' \to \gamma\chi_j$, and $\chi_j \to \gamma J/\psi$ transitions D is pure dipole, Q is pure quadrupole, D+Q is equal mixture with positive relative sign, D-Q is equal mixture with negative relative sign. The likelihood products for the data samples shown behave gaussianly in the region of the peaks; we thus plot contours of the likelihood function in 1 σ cells, with each cell below the main peak corresponding to successive 1 σ deviations from the best estimate. The results obtained ar- compatible with dipole dominance. See reference 38 for details.

state	$\Gamma(\chi \to a^1 1)$	$\Gamma \cdot \Gamma(CB)_{exp}$ $(KeV)^2 \times 10^2$	$\Gamma \cdot \Gamma(CCM)_{th}$ $(KeV)^2 \times 10^2$
2^3P_0	≈10±4 MeV	20±8	56
2^3P_1	<2	<102	87
2^3P_2	3±1	81±33	84

Table 7. Comparison of experiment [33,38] to theory[42] of the γ cascade transition rates. We use $\Gamma_{\psi'} = 215 \pm 40$ KeV[17].

Agreement is surprisingly good given the non-relativistic approximations which have been made in the CCM.

Given the results for the first γ transition rates the agreement seen in table 7 is probably an accident. Results published in 1977 from the MP^2S^3D collaboration[43] for the first γ transition rates are,

$$\left.\begin{aligned} \Gamma(\psi' \to \gamma\chi_0) &= 15.5 \pm 5.0 \text{ KeV} \\ \Gamma(\psi' \to \gamma\chi_1) &= 15.3 \pm 4.1 \text{ KeV} \\ \Gamma(\psi' \to \gamma\chi_2) &= 15.0 \pm 4.3 \text{ KeV} \end{aligned}\right\} \pm 19\% \text{ (systematic error) (from } \Gamma_{\psi'} \text{ uncertainty)} \quad \text{(III-66)}$$

Again, using $\Gamma_{\psi'}$=215±40KeV.

New, preliminary numbers from the Crystal Ball Collaboration are discussed in detail in reference 33,

$$\left.\begin{aligned} \Gamma(\psi' \to \gamma\chi_0) &= 20.8 \pm 1.3 \pm 3.4 \text{ KeV} \\ \Gamma(\psi' \to \gamma\chi_1) &= 18.9 \pm 1.1 \pm 3.0 \text{ KeV} \\ \Gamma(\psi' \to \gamma\chi_2) &= 16.6 \pm 1.1 \pm 2.5 \text{ KeV} \end{aligned}\right\} \pm 19\% \text{ (systematic error) (from } \Gamma_{\psi'} \text{ uncertainty)} \quad \text{(III-67)}$$

when the first error shown is point to point and the second is an overall systematic uncertainty.

The agreement between the old and new experimental results is within the relative systematic errors (excluding the overall error on the $\Gamma_{\psi'}$); however, the Crystal Ball numbers tend to be larger. Within the point to point errors there is an indication for an increase in rate from χ_2 to χ_0 transitions for the Crystal Ball data. Since,

$$\Gamma(\psi' \to \gamma\chi_j) \propto (2j_f+1)\omega_j^3, \qquad \text{(III-68)}$$

c.f.(III-34), we expect,

$$\Gamma(\psi' \to \gamma\chi_0)/\omega_0^3 : \Gamma(\psi' \to \gamma\chi_1)/3\omega_1^3 : \Gamma(\psi' \to \gamma\chi_2)/5\omega_2^3 = 1:1:1 \qquad \text{(III-69)}$$

The Crystal Ball experiment yields: $1 \pm 0.07 : 1.05 \pm 0.08 : 1.37 \pm 0.11$. However, as table 8 shows, the absolute comparison is somewhat worse.

state	Theory(CCM)	Exp. (± full error)
$\Gamma(\psi' \to \gamma\chi_0)$	43 KeV	20.8±4.5 KeV
$\Gamma(\psi' \to \gamma\chi_1)$	34	18.9±3.9
$\Gamma(\psi' \to \gamma\chi_2)$	24	16.6±3.6

Table 8. Comparison of the absolute rates for $\psi' \to \gamma\chi_j$. Theory is reference 42, experiment is from reference 33. The full systematic errors of the experiment have been included for this comparison.

The M1 transitions should be easier to calculate since $M_{ij} \approx 1$ (c.f.(III-37)), (only spin flip is involved),

$$\Gamma(n^3S_1 \to n^1S_0)/\omega_n^3 \approx 16/3(Qc/2M_c)^2 \approx 1275\ \text{KeV}/(\text{GeV})^2\text{(CCM)} \qquad \text{(III-70)}$$

Thus, using $\omega_1 = 111 \pm 5$ MeV, and (III-54),

$$Br_{th}(J/\psi \to \gamma\eta_c) \approx (2.6 \pm 0.5)\% \qquad \text{(III-71)}$$

The Crystal Ball has measured this branching ratio[33] to be,

$$Br_{exp}(J/\psi \to \gamma\eta_c) = (1.20\ ^{+0.53}_{-0.35})\% \qquad \text{(III-72)}$$

Thus again, the agreement between the CCM and experiment is reasonable given the limitations of the model.

We may conclude after our somewhat cursory comparison of the charmonium model to experiment (actually only two or three non-relativistic models were compared), that agreement is suprisingly good considering the approximations made in the models. The charmonium system does have important relativistic corrections, and higher order QCD corrections[33]. However, the bottomonium system should be better in these respects and theory awaits crucial tests as the exploration of this unique system progresses.

IV. What is left to learn?

a) Questions about Bottom

As we saw in Section II, bottomonium is quite non-relativistic with $\langle v^2 \rangle \approx 0.08$. Thus we expect to learn a great deal about quark dynamics through the careful observation of the bottomonium system. In particular, the following topics should prove to be illuminating.

- Leptonic widths
- n^3S_1 mass splitting
- 2^3P_j cog
- 2^3P_j fine structure and classification
- $\Gamma(\Upsilon' \to \gamma^3P_j)$
- $\Upsilon - \eta_b$ mass splitting

a) The discovery of the Υ system:

The Υ was discovered at Fermilab using the process. $P + Be \to \mu^+\mu^- + X$. Figure 20 shows the results from Fermilab and the confirming results from DORIS I.

Figure 21 shows results from the Cornell storage ring CESR, on the Υ system.

The rates for Υ system production in e^+e^- collisions are considerably smaller than in the J/ψ system case, and thus make the Υ system much more difficult to study. This is due to a number of factors. Considering the case of the Υ', first, $\sigma(e^+e^- \to \Upsilon') \propto Q_b^2/m_\Upsilon^2$, which drops the cross section by a factor of ≈ 36 from the

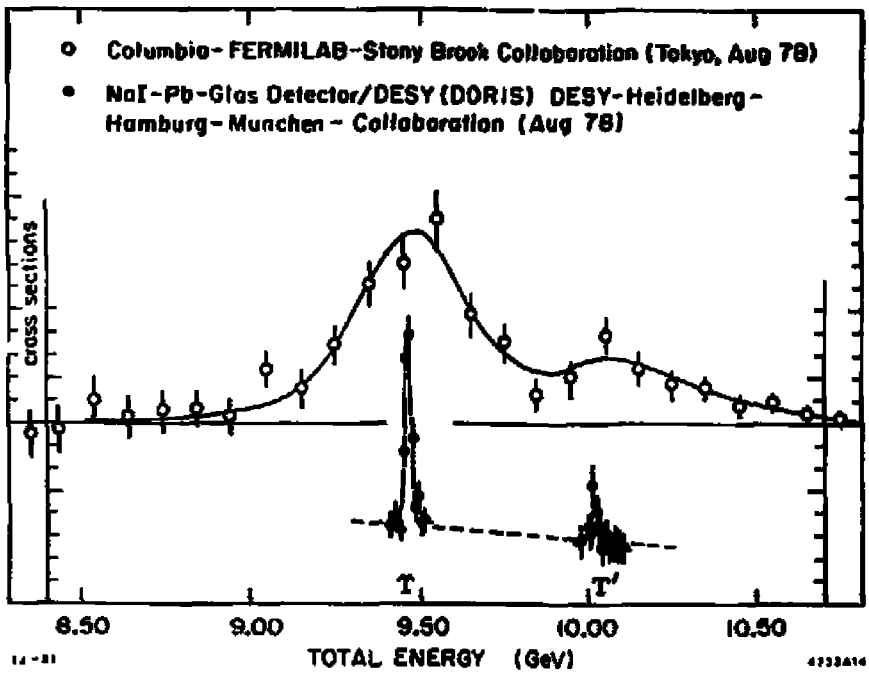

Figure 20. Columbia-Fermilab-Stony Brook and DESY-Hamburg-Heidelberg-Muenchen Collaborations: The Υ family produced in hadronic and e^+e^- reactions.

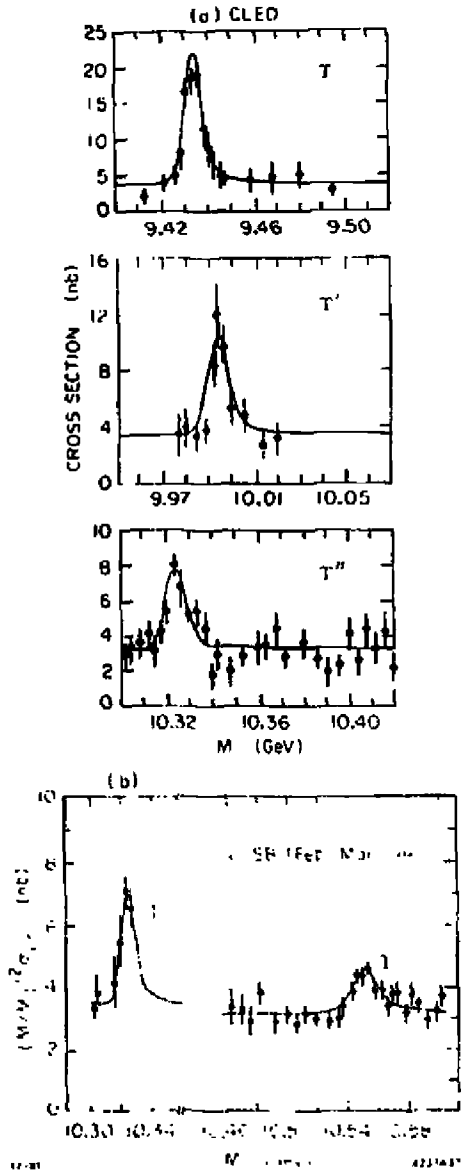

Figure 21. a) The Υ, Υ' and Υ'' states observed in e⁺e⁻ reactions at CESR using the CLEO magnetic detector[59]. b) The Υ'' and Υ''' states observed at CESR using the CUSB NaI(Tℓ) detector[65]. Note that the Υ''' is wider than the machine resolution signaling the production of B(B) mesons.

ψ'. Second,

$\sigma(e^+e^- \to \Upsilon) \propto 1/\Delta E_{beam}$, where ΔE_{beam} is the energy spread of the storage ring. For SPEAR and DORIS (both machines have about the same magnetic radius),

$$\Delta E_{beam} \propto 2\times10^{-3} E_b^2 \text{ (GeV)}. \qquad \text{(IV-1)}$$

Thus SPEAR at the ψ' gains another factor of $\propto 7$ over DORIS at the Υ' due to the beam energy resolution, and so a total factor of about 250 is lost. All is not lost however, DORIS II[56] has a much greater luminosity at the Υ' than SPEAR has at the ψ', and the production rate is proportional to the luminosity. About a factor of 10 more integrated nb^{-1}/day is expected for DORIS II at the Υ' as compared to SPEAR at the ψ'. At SPEAR about 20k ψ' events are collected per day. Thus at DORIS II we expect about 800 Υ' events/day. Note that CESR should also collect about 800 Υ' events/day. The luminosity of CESR is lower than DORIS II at the Υ', but the machine energy resolution is about a factor of two smaller due to the greater magnetic radius of the machine.

What is obviously needed is a machine with 10 times more luminosity. Machine physics is a growth industry!

b) Leptonic widths and the determination of Q_b.

Figure 22 shows $\Gamma(1^3S_1 \to e^+e^-)$, equation III-33, divided by the square of the average quark charge, e.g., for the ρ, $(\Sigma C_i Q_i)^2 = (1/\sqrt{2}\ 2/3 + 1/\sqrt{2}\ 1/3)^2 = \frac{1}{2}$.

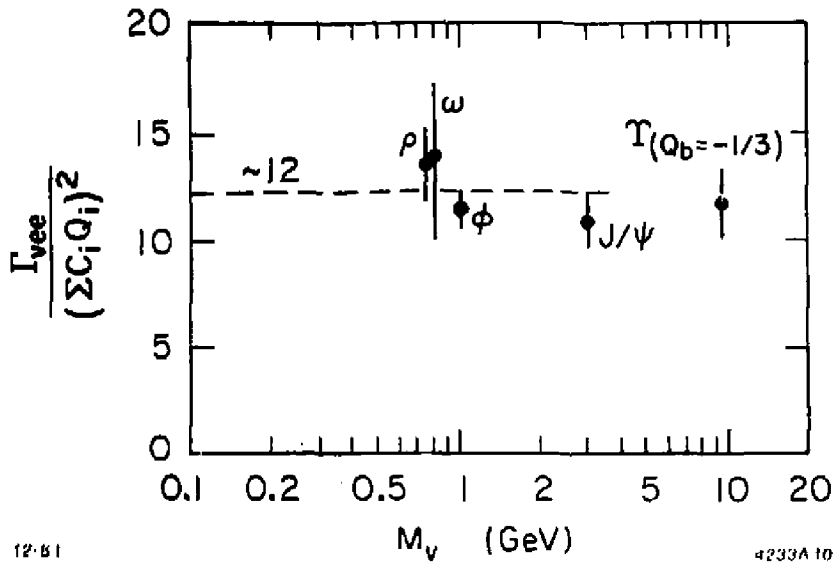

Figure 22. The leptonic decay widths of the 1^3S_1 vector mesons divided by the square of the average quark charge as a function of the meson mass.

As is seen from the figure, and using (III-33),

$$\frac{\Gamma(1^3S_1 \to e^+e^-)}{4\alpha^2(\Sigma Q_i C_i)^2} = \frac{|R(0)|^2}{M(^3S_1)^2} \simeq 5.6\times10^{-4} \quad \text{(IV-2)}$$

for the mesons with mass below the Υ. On choosing $Q_b^2 = 1/9$, we find

$$|R_\Upsilon(0)|^2/M_\Upsilon{}^2 \simeq 5.4\times10^{-4}. \quad \text{(IV-3)}$$

while $Q_b^2 = 4/9$ yields a value 4 times smaller. Thus it is natural to assign $Q_b = -1/3$. There are more sophisticated arguments[57] based on potential models which support the 1/3 assignment; however, these depend on general assumptions about the nature of the $b\bar{b}$ potential. Measurements[58] of R_{had} for $E_{cm} < M_\Upsilon'''$, and $E_{cm} > M_\Upsilon'''$ also confirm consistency with $Q_b = -1/3$. It is interesting to note the regularity for $|R(0)|^2$ implied by equation (IV-2). No commonly accepted potential is able to reproduce this simple relation; indeed, due to the involvement of the ρ ω and ϕ its explanation is somewhat mysterious.

c) The mass splitting of the n^3S_1 states.

Initial predictions[59] of the $M_\Upsilon' - M_\Upsilon = \Delta M_\Upsilon$ used the standard potential of section III,

$$V(r) = \kappa/r + r/a^2 \quad \text{(IV-4)}$$

where the $M_{\psi'} - M_{J/\psi}$ was used as input and no "flavor tuning" of the potential was attempted. These initial predictions gave values of ΔM_Υ 30 to 80 MeV smaller than the experimental values. This failure of the potential (IV-4) led to the development of a series of potentials with considerably different asymptotic characteristics all of which are able to reproduce the observed $\Delta M_\Upsilon = 560\pm3$ MeV, as well as the other n^3S_1 masses for the Υ system (c.f. figures 4 and 5). The

characteristics of these recent potentials are reviewed in detail in reference 18c. Briefly, the reason that potentials with such diverse asymptotic behaviors are able to reproduce the n^3S_1 mass splitting is that much of the bound state wave function is located at values of r where V(r) is neither dominated by 1/r or r behavior. As is shown in figure 23, the average radii of the states studied lie in the region of transition between the two postulated asymptotic behaviors.

d) The center of gravity (cog) of the masses of the n^3P_j states.

The potentials which are now used to describe quarkonium are clearly not coulombic in the region of greatest influence on the system. Thus the original motivation of Appelquist and Politzer in predicting bound states, and the analogy to positronium, has been somewhat blurred. In particular, the n^2 energy degeneracy of the coulombic central potential, which gives the n^3S_1 and n^3P_j states the same mass, is no longer true. All recent models predict a shift in the mass of the n^3P_j cog with respect to the n^3S_1 without including a spin-orbit interaction, where.

$$M(n^3P_j)_{cog} = 1/9\sum_{j=0}^{2}(2j+1)M(n^3P_j). \qquad \text{(IV-5)}$$

e) n^3P_j fine structure and classification

The fine structure for the quarkonium system, in the present models, does not shift the cog of the P states (which is not the case for positronium). For simple potentials, the fine structure mass splitting terms scale like[7]

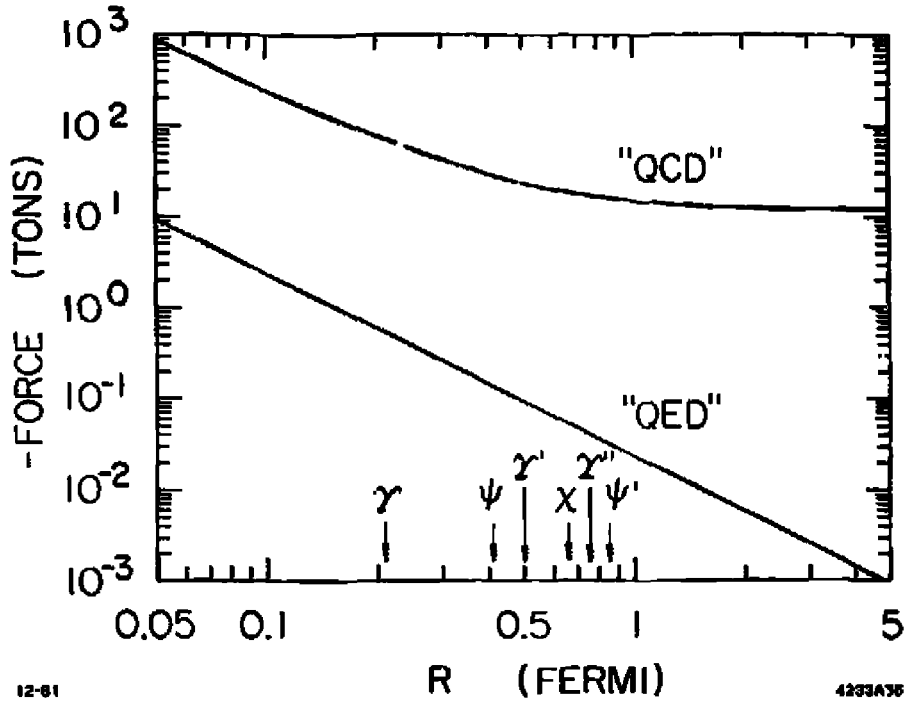

Figure 23. Force [Tons] vs r [Fermi] for the coulomb force (lower curve), and the Richardson potential[18]. The mean square radii for the J/ψ, ψ', Υ, and Υ' are also shown. See reference 18c for an in depth discussion of the properties of many of the potentials.

$$(1/M_q^2)\,(d^2V/dr^2) + (1/M_q^2 r)\,(dV/dr) \propto M_q^{-[2\nu+2]/[\nu+2]} \qquad \text{(IV-6)}$$

where,

$$V = \pm\, a r^{\nu}, \text{ (-a for } \nu < 0). \qquad \text{(IV-7)}$$

Thus, for a coulombic potential, $V \propto 1/r$ we find $\Delta M_{f-s} \propto M_q^{-5/3}$, while for $\nu = 0$ ($\log(r/r_0)$), $\Delta M_{f-s} \propto M_q^{-1}$.

Experimentally determining $M(n^3P_j)_{cog}$ and ΔM_{f-s} is thus an important check of the general characteristics of the quarkonium potential models.

Of course before a detailed comparison can be made, the j^P of the χ_b states must be determined. In principle, this can be accomplished the same way it was for the χ_c states, e.g., for n = 2,

$$\Upsilon' \to \gamma\chi_b \to \gamma\gamma\Upsilon \to \gamma\gamma\ell^+\ell^- \qquad \text{(IV-8)}$$

can be analyzed to obtain j, while the exclusive hadronic decays of the χ_b states can be examined to determine P. However, as we shall discuss, the branching ratio for the process (IV-8) is projected to be quite a bit lower than for the J/ψ system, and as we have seen, the Υ' production rate is much lower than the ψ' production rate. Also the average charge multiplicity, $\langle n\rangle_c$, is $\langle n\rangle_c \approx 8$ at the Υ', while $\langle n\rangle_c \approx 4$ at the ψ'. The expected branching fraction into $\pi\pi$ or KK for the $j^P = 0^+, 2^+$ states, is thus substantially lower for the χ_b states as compared to the χ_c states. Thus the prognosis is for rather slow progress on these questions, unless some suprises are in store. I expect that substantial information about even the simplest quantity to measure, $M(2^3P_j)_{cog}$, will be two years in coming, i.e., the summer of 1983.

f) Branching ratios for $\Upsilon' \to \gamma\chi_{bj}$, and the γ cascade reactions.

Many theoretical estimates have been made for the partial widths, $\Gamma(\Upsilon' \to \gamma\chi_{bj})$ for bottomonium[16]. In order to obtain branching ratios the full width of the Υ' is also needed. There has been some uncertainty in $\Gamma_{\Upsilon'}$ due to lack of knowledge of the $\pi\pi$ transition from the Υ' to the Υ. Theoretically[50],

$$\frac{\Gamma(\psi' \to J/\psi\pi\pi)}{\Gamma(\Upsilon' \to \Upsilon\pi\pi)} \approx \left[\frac{\langle r_{\psi'}^2 \rangle}{\langle r_{\Upsilon'}^2 \rangle}\right]^2 \approx 10. \qquad (IV-9)$$

if the gluon has spin 1. Thus the accuracy of this prediction is crucial in the theoretical determination of $\Gamma_{\Upsilon'}$. In the case of the ψ', $\Gamma(\psi' \to \pi\pi) = \frac{1}{3}\Gamma_{\psi'}$. Recently the LENA collaboration at DORIS reported[51] the first measurement of $Br(\Upsilon' \to \pi^+\pi^-\Upsilon)$. Measurements of this branching rati have also been made by the CLEO[52] and CUSB[53] detectors at the CESR storag ring. The average of the three measurements yield, assuming isotopic spi invariance in the decay,

$$Br(\Upsilon' \to \pi\pi\Upsilon) = (28.8 \pm 3.9)\% . \qquad (IV-10)$$

In order to obtain $\Gamma_{\Upsilon'}$, the LENA group had to use a complex argument since a direct measurement of $\Gamma_{\Upsilon'}$ has not yet been accomplished due to th large amount of running time needed. Let us now make a slight diversion and reproduce the LENA argument here; its validity saves a lot of machine time.

$$\Gamma_{\Upsilon'} = \Gamma(\Upsilon' \to 3g(\text{hadrons})) + \Gamma(\Upsilon' \to 2g\Upsilon(\pi\pi\Upsilon)) + \sum_{j=0}^{2} \Gamma(\Upsilon' \to \gamma\chi_{bj}) + \Gamma_{em}(\Upsilon' \to \text{hadrons}) \qquad (IV-11)$$

also,

$$\Gamma_{\Upsilon} = \Gamma(\Upsilon \to 3g\ (\text{hadrons})) + \Gamma_{em}(\Upsilon \to \text{hadrons}) \qquad (IV-12)$$

where Γ_{em} is the process shown in figure 24.

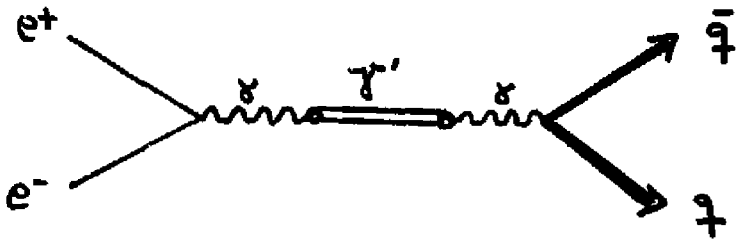

Figure 24.The diagrammatic representation of the process which yields Γ_{ee}.

Both Γ_{3g} and Γ_{qq} are proportional to Γ_{ee} (for the Υ, $\Gamma_{ee}(\Upsilon) \equiv \Gamma(\Upsilon \to e^+e^-)$),

and,

$$(\Gamma_\Upsilon/\Gamma_{ee}(\Upsilon)) \propto (\Gamma(\Upsilon' \to 3g) + \Gamma_{qq}(\Upsilon' \to \text{hadrons}))/\Gamma_{ee}(\Upsilon') \qquad \text{(IV-13)}$$

letting,

$$B_{ee}(\Upsilon) \equiv \Gamma_{ee}(\Upsilon)/\Gamma_\Upsilon \qquad \text{(IV-14)}$$

we find,

$$\Gamma(\Upsilon' \to 3g) + \Gamma_{qq}(\Upsilon' \to \text{hadrons}) = \Gamma_{ee}(\Upsilon')/B_{ee}(\Upsilon) \qquad \text{(IV-15)}$$

also[59],

$$\Gamma(\Upsilon' \to 2g\Upsilon) = Br(\Upsilon' \to \pi\pi\Upsilon)\Gamma_{\Upsilon'} \qquad \text{(IV-16)}$$

combining, (IV-11), (IV-15), and (IV-16), we obtain,

$$\Gamma_{\Upsilon'} = \frac{[\Gamma_{ee}(\Upsilon')/B_{ee}(\Upsilon) + \sum_{j=0}^{2}\Gamma(\Upsilon' \to \gamma\chi_{bj})]}{1 - Br(\Upsilon' \to \pi\pi\Upsilon)} \qquad \text{(IV-17)}$$

using the LENA values for[54]

$$\Gamma_{ee}(\Upsilon') = (0.56 \pm 0.09)\ \text{KeV} \qquad \text{(IV-18)}$$

and[61]

$$B_{ee}(\Upsilon) = (3.2 \pm 0.8)\% \qquad \text{(IV-19)}$$

we obtain,

$$\Gamma_{ee}(\Upsilon')/B_{ee}(\Upsilon) = 18^{+6}_{-5}\ \text{KeV} \qquad \text{(IV-20)}$$

and finally,

$$\Gamma_{\Upsilon'} = 26 \pm 9\ \text{KeV} + (1.42 \pm 0.02)\sum_{j=0}^{2}\Gamma(\Upsilon' \to \gamma\chi_{bj}) \qquad \text{(IV-21)}$$

The width of the Υ has been obtained[55],

$$\Gamma_\Upsilon = 40\ ^{+13}_{-8}\ \text{KeV}.$$

In order to estimate the effect of the γ transitions, we can use scaling laws[7] using (III-34),

$$\Gamma(\Upsilon' \to \gamma\chi_{bj})/\Gamma(\psi' \to \gamma\chi_{cj}) =$$

$$(Q_b/Q_c)^2(\omega_{bj}/\omega_{cj})^3\ |E_{if}|_b^2/|E_{if}|_c^2 \qquad \text{(IV-22)}$$

For a potential of the form (IV-7),

$$(\omega_{bj}/\omega_{cj})^3\ |E_{if}|_b^2/|E_{if}|_c^2 \propto (m_b/m_c)^{-3\nu+2/(\nu+2)} \qquad \text{(IV-23)}$$

Then, for $\nu \to 0$ ($\log(r/r_0)$),

$$\Gamma(\Upsilon' \to \gamma\chi_{bj}) \simeq (1/4)(1/3)\Gamma(\psi' \to \gamma\chi_{cj}) \qquad \text{(IV-24)}$$

and[33],

$$\sum_{j=0}^{2} \Gamma(\psi' \to \gamma\chi_{cj}) \simeq 60\ \text{KeV} \qquad \text{(IV-25)}$$

and so,

$$\sum_{j=0}^{2} \Gamma(\Upsilon' \to \gamma\chi_{bj}) \simeq 5\ \text{KeV} \qquad \text{(IV-26)}$$

using this value,

$$\Gamma_{\Upsilon'} \simeq 33 \pm 10\ \text{KeV} \simeq \Gamma_{\Upsilon}. \qquad \text{(IV-27)}$$

This is certainly not the case in the J/ψ system where $\Gamma_{\psi'} \simeq 3\Gamma_{J/\psi}$. Of course the relatively narrower width of the Υ' as compared to the ψ' is an important boost to the observation of the γ lines, since their observation rate is proportional to $Br(\Upsilon' \to \gamma\chi_{bj})$. We can estimate using (IV-26) and (IV-27),

$$\sum_{j=0}^{2} Br(\Upsilon' \to \gamma\chi_{bj}) \simeq 15\%. \qquad \text{(IV-28)}$$

How such lines would appear in the Crystal Ball Detector using 125k Υ' decays is shown using a Monte Carlo simulation[56] in figure 25.

Figure 26 shows the data sample obtained for the γ cascade process using a different Monte Carlo model[56], and a different theoretical model[56], than used for figure 25. 120 cascade events are obtained from 125 k Υ' decays

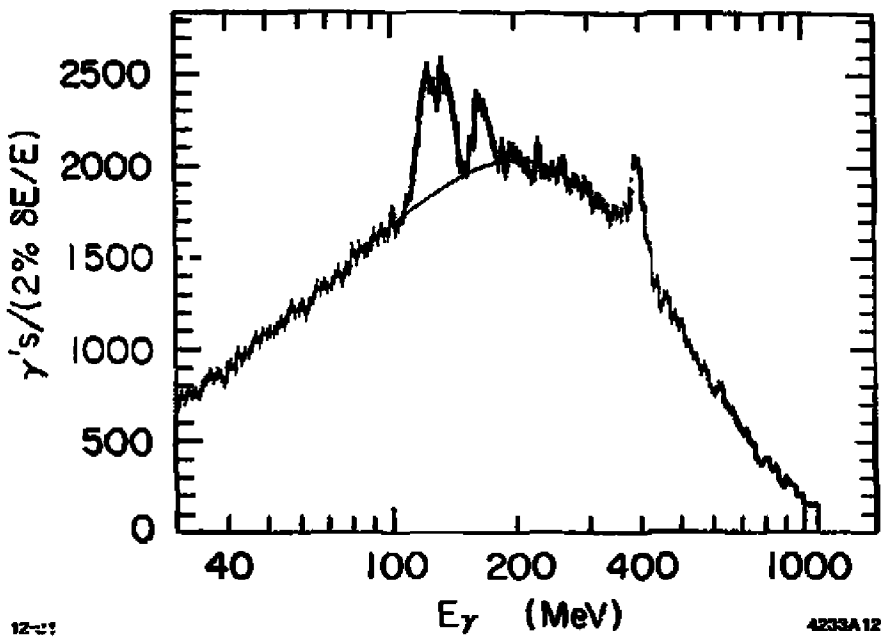

Figure 25. A Monte Carlo simulation of the Υ′ inclusive γ spectrum in the Crystal Ball Detector. 125k Υ′ decays are shown. Acceptance cuts, pattern and overlap cuts and a π^0 subtraction are in the Monte Carlo as described in reference 56. The model of Quigg and Rosner was used[57], which has $Br(\Upsilon' \to \gamma\chi_{b2}) = 8\%$, $Br(\Upsilon' \to \gamma\chi_{b1}) = 6.0\%$, and $Br(\Upsilon' \to \gamma\chi_{b0}) = 4.3\%$.

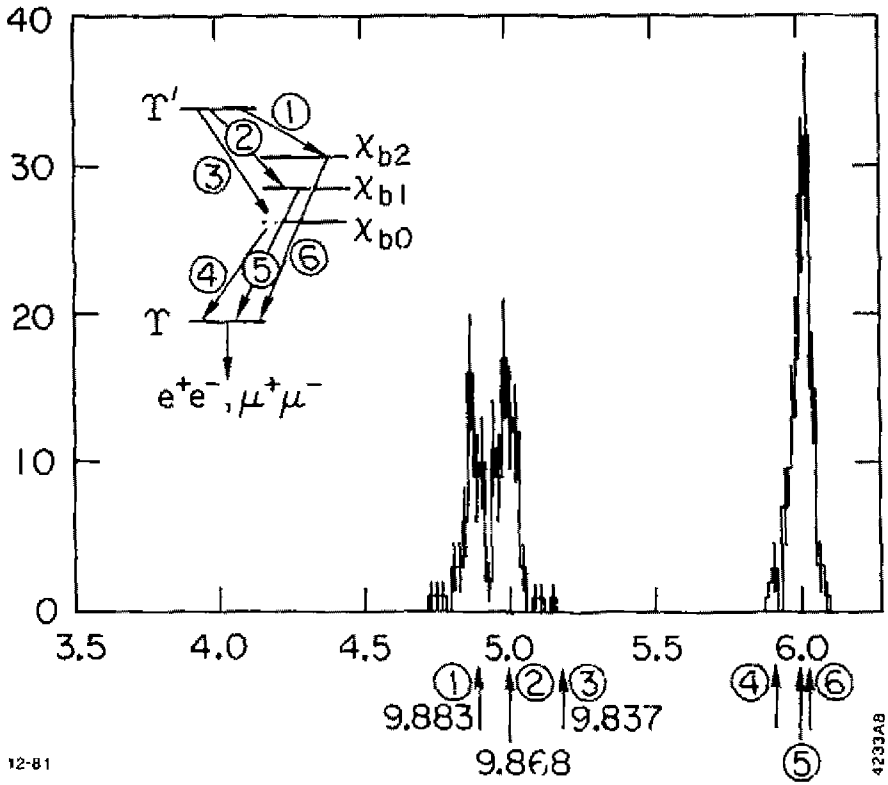

Figure 26. A Monte Carlo simulation of the γ cascade process from the decay of 125k Υ′ in the Crystal Ball Detector. A diagrammatic representation of the cascade is shown at the upper left of the figure.

after all cuts. Two or three times this data sample (two or three years of running at DORIS II) would allow a spin analysis to determine the j of the states. Thus the prospects look reasonable that within the next three to four years many of the interesting questions we have pondered in this section will have substantial experimental input.

g) Hyperfine Splitting, the η_b.

Estimates for the η_b mass[16] place it about 46 MeV below the Υ. Given the ω^3 factor in the formula for the M1 transition, (III-36), the rate will be highly suppressed. Also, the observation of a $\approx$ 50 MeV photon in the large backgrounds present around that energy in the Υ inclusive γ spectrum makes the measurement extremely difficult. It thus seems that the most likely way to observe the η_b is through the hindered M1 transition, where the photon has about a 600 MeV energy. Of course this possibility depends on how hindered the transition actually turns out to be.

V. On to top.

Figure 27 shows a recent compilation of threoretical predictions as to where $t\bar{t}$ threshold is to be found. Within two years PETRA will have extended its energy to well over $E_{cm} \approx 40$ GeV. Is there life beside the Z^0?

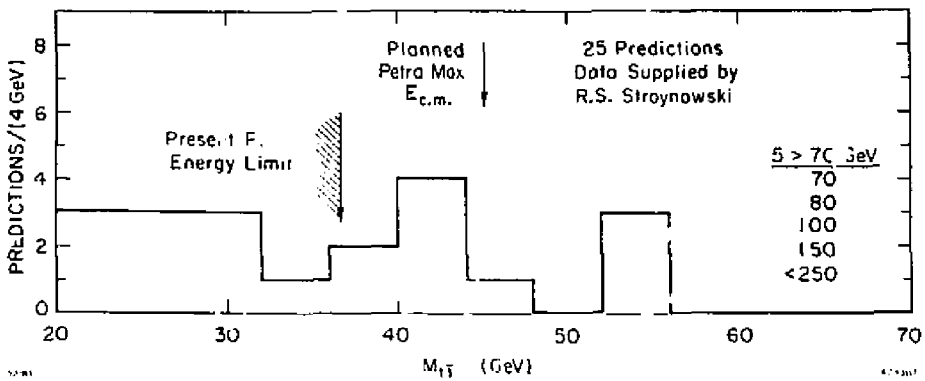

Figure 27. $M_{t\bar{t}}$ vs # Predictions/4GeV.

REFERENCES

1. Most recent limit from a number of PETRA experiments.

2. S. L. Glashow, J. Iliopoulos, L. Maini, Phys. Rev. D, 2, p.1285 (1970).

3. H. Harari, Proceedings of SLAC Summer Institute, SLAC Report #204,p.204, Editor M.C.Zipf, (1977)

4. R. J. Cashmore, Lectures given at 16th International School of Elementary Particle Physics, Kupui, Yugoslavia, Oxford University Nuclear Physics Laboratory Report #14/81, (1981).

5. J. J. Sakurai, Advanced Quantum Mechanics (Addison Wesley, New York, 1961).

6. R. L. Jaffe and F. E. Low, Phys. Rev. D, 19, p.2105 (1979).

7. T. Sterling, Nuc. Phys. B 141, p.272 (1978).

8. J. L. Richardson, Phys. Lett. B 82, p.272 (1979).

9. S. Mohorovicic, Astr. Nachr. (Berlin), 253, No. 6052, p.93, (1934).

10. M. Deutch, Phys. Rev. 82, p.455 (1951).

11. A. P. Mills Jr., S. Berko, and K. F. Canter, Phys. Rev. Lett. 34, p.1541 (1975).

12. T. Fulton and P. C. Martin, Phys. Rev. 95, p.811 (1954).

13. H. Grotch and D. R. Yennie, Rev. Mod. Phys. 41, p.350 (1969).

14. S. Brodsky, private communication.

15. An excellent recent review of Positronium Research is in, A. Rich, Rev. Mod. Phys. 53, p.127 (1981).

16. For comprehensive reviews, see:

    a) T. Appelquist, A. M. Barnett, K. Lane, Ann. Rev. of Nucl. and Part. Sci. 28, p.387 (1978); b) M. Krammer and H. Krasemann, DESY Report 79/20, (1979);
    c) W. Buchmuller, S.-H.H.Tye, Phys. Rev. D24, p.134 (1981).

17. Particle Properties Data Booklet, Rev. Mod. Phys. 52, (1980).

18. G. Bellettini, et al., Nuovo Cim. 66A, p.243 (1970); V.I. Kryshki et al., J. Exp. Theor. Phys. 30, p.1037 (1970); A. Browman et al., Phys. Rev. Lett. 33, p.1400 (1974).

19. E.D.Bloom, Proceedings of the XVIth Recontre de Moriond, Les Arcs, France, March 15-27, 1981 (1982); also SLAC-Pub-2779 (1981).

20. R. M. Barnett, M. Dine and L. McLerran, Phys. Rev. D 22, p.594 (1980).

21. R. M. Barnett, private communication.

22. M.B.Atwood, Proceedings of the Summer Institute on Particle Physics, SLAC Report #224, p1, Editor A. Mosher (1980).

23. M. Chanowitz, Proceedings of the SLAC Summer Institute on Particle Physics, SLAC Report #245, Editor A. Mosher (1982).

24. G. Wolf, DESY Report 80/85 (1980).

25. J. D. Jackson, Proceedings of the SLAC Summer Institute, SLAC Report #198, p147, Editor M.C.Zipf (1976).

26. T. Appelquist, H. D. Politzer, Phys. Rev. Lett. 34, p.34 (1975).

27. J. J. Aubert, et al., Phys. Rev. Lett. 33, p.1404 (1974).

28. J. E. Augustin, Phys. Rev. Lett. 33, P.1406 (1974).

29. G. Feldman, Proceedings of the SLAC Summer Institute on Particle Physics, SLAC Report #196, p81, Editor M.C.Zipf (1976).

30. G. Goldhaber, et al., Phys. Rev. Lett. 37, p.225 (1976).

31. R. Partridge, et al., Phys. Rev. Lett. 45, P.1150 (1980).

32. C. Edwards, et al., SLAC-Pub-2814, (submitted to Phys. Rev. Lett.) (1981).

33. F. Porter, Invited talk, SLAC Summer Institute on Particle Physics, SLAC Report #245, Editor A. Mosher (1982), SLAC-Pub-2796 (1980).

34. W. Braunschweig, et al., Phys. Lett. 67B, p.243 (1977).

35. R. Partridge et al., Phys. Rev. Lett. 45, p.959 (1980).

36. M. A. Schifman, A. I. Vainshtein, M. B. Voloshin and V. I. Zakharov, Phys. Lett. 77B, p.80 (1978).

37. G. Karl, S. Meshkov and J. Rosner, Phys. Rev. D 13, p.1203 (1976).

38. M. J. Oreglia, PhD. thesis, Stanford University, SLAC Report #226 (1980).

39. T. M. Himel, Ph.D. Thesis, Stanford University, SLAC Report #223 (1979).

40. T.Appelquist, et al., Phys. Rev. Lett. 34, p.365 (1975); C. G. Callan, et al., Phys. Rev. Lett. 34, p.52 (1975); M. Chanowitz, Phys. Rev. D 12, p.918 (1975); L. Okun, M. Voloshin, Moscow Report ITEP-95-1976 (1976); S. J. Brodsky et al., Phys. Lett. 73B, p.203 (1978).

41. W. Buchmuller, et al., CLNS 81/497 and Fermilab-Pub-81/46-THY (1981).

42. E. Eichten et al., Phys. Rev. D21, p.203 (1980).

43. C. J. Biddick et al., Phys. Rev. Lett. 38, p.1324 (1977).

44. D. Andrews et al., Phys. Rev. Lett. 44, p.1108 (1980); D. Andrews et al., Phys. Rev. Lett. 45, p.219 (1980).

45. T. Bohringer et al., Phys. Rev. Lett. 44, p.1111 (1980); G.Finocchiaro et al., Phys. Rev. Lett. 45, p. 222 (1980).

46. K. Wille, DESY Report 81-047 (1981).

47. J. L. Rosner, C. Quigg and H. B. Thacker, Phys. Lett. 74B, p350 (1978).

48. J. Lee-Franzini, Cornell Report No. CLNS 81/488, Submitted for Publication to Surveys High Energy Phys., (1981).

49. E. Eichten, et al., Phys Rev. D17, p3090 (1978).

50. K. Gottfried, Phys. Rev. Lett., 40, p598 (1978); T. M. Yan, Phys. Rev. D22, p1652 (1980).

51. B. Niczyporuk, et al., Phys. Lett. 100B, p95 (1981).

52. J. J. Muller et Al., Phys. Rev. Lett. 46, p1181 (1981).

53. D. Mageras et al., Phys. Rev. Lett. 46, p1115 (1981).

54. B. Niczyporuk, et al., Phys. Lett. 99B, p169 (1981).

55. H. Schoder, DESY Report 80/61 (1980).

56. Crystal Ball Collaboration, Proposal for Investigating $b\bar{b}$ Spectroscopy at DORIS II Using the Crystal Ball, DESY PRC 81/09, (1981).